Bard

Spring 2021

Detection of C-Reactive Protein Using an ELISA Immunodot as a Proof-of-Concept for Paper Microfluidics

Frank J. Rybicki IV
Bard College, fr5492@bard.edu

Recommended Citation

Bard

Detection of C-Reactive Protein Using an ELISA Immunodot as a Proof-of-Concept for
Paper Microfluidics

Senior Project submitted to

The Division of Science, Mathematics, and Computing
of Bard College

by

Frank Rybicki

Annandale-on-Hudson, New York
May 2021

Acknowledgements

I would like to thank the Bard Chemistry Department for nurturing my love of science and my passion for experiments. Specifically, I would like to thank Professor Lafratta and Professor Jain for making my project possible and helping me to troubleshoot and regroup after my more ambitious goals proved technically impossible for me. This project taught me scientific humility and was an important part of my professional growth. I also want to thank Professor McLaughlin for being a constant support for my academic and athletic aspirations.

I hope that my work in this thesis can live up to the high expectations for scholarship that I put onto myself on a daily basis. Despite the relative – on the "surface" simplicity of this project, the results and implications are meaningful to me and I hope that the extensive research is well-received in such a short treatise. I also hope to conduct future research on paper microfluidics because the field is rapidly expanding and will continue to play a key role in future diagnostic testing. The COVID-19 pandemic demonstrated the high utility of paper analytics and hopefully these devices continue to play a key role in public health.

I would also like to thank my parents, my baseball teammates, and my extended family for the opportunity to be a student-athlete and from an academic perspective to remain curious and diligent. Coaches Andy Salvatore, Jesse Marsh, and Justin Gomez have been key role models in my college maturation.

Table of Contents

Abstract

Medicine relies heavily on diagnostic testing. Before the end of 2019 – the beginning of 2020, the modernized world took for granted accurate and available diagnostic tests. The COVID-19 pandemic taught the world, even the wealthiest countries, how fragile human health can become when tests are lacking. The assumption of available testing and the confidence in test results has been seriously challenged. With these challenges, Point-of-Care (PoC) tests has transgressed medicine and science to include politics, finance, and humanity at its core. This Bard senior project is rooted in the science of a proof-of-concept paper-based ELISA Immunodot assay for the detection of C-reactive protein (CRP). CRP can be identified at varying blood concentrations found in humans physiology and disease. CRP testing is used for clinical diagnoses millions of times per month in the United States. The results confirm that the ELISA Immunodot can both distinguish CRP+ and CRP- standards and semi-quantitively predict the CRP concentration of the standard. The ability to relate the intensity of the CRP colorimetric output to a standard CRP concentration has potential applicability in future medical testing.

1. Introduction

1.1 Diagnostic testing

A vast array of tests are essential to healthcare. Data provided from these tests supplement the data that doctors and other healthcare providers acquire from a History and Physical (H&P) examination. One key principle in medical education is that providers use the H&P to arrive at a differential diagnosis. This list orders the most likely diagnosis first and ranks the lower likelihood diagnoses with respect to probability.

For example, consider a patient who presents with joint pain. A hypothetical differential diagnosis for his or her condition could be osteoarthritis (a degenerative disease) or rheumatoid arthritis (an inflammatory disease). The H&P will include factors related to the presentation of the condition (is the pain localized to one joint or does the condition affect multiple joints?) and features (does the patient experience a sharp or dull pain? Is the pain constant? Is the pain more intense in the morning?). The differential diagnosis rank order includes these factors as well as patient demographics such as age, sex, prior medical history, and family history.

For this hypothetical patient, two major groups of diagnostic tests will refine, narrow, and ultimately help make a single, accurate diagnosis. Making the correct diagnosis is critical because the disease progression and treatment is different for each scenario. The first group is medical imaging. Medical imaging (radiography, computed tomography, and magnetic resonance Imaging) can refine the differential diagnosis by examining the anatomy and pathology of the diseased area. In some cases, such as with a bone fracture, a medical imaging study is the only diagnostic test needed to make

an accurate diagnosis. However, for this hypothetical patient, osteoarthritis and rheumatoid arthritis have overlapping features on radiographs and therefore, the test is nonspecific.

The second group of diagnostics following the H&P is blood laboratory testing. The biomarker profile will determine if the diseased joint(s) seen on the imaging studies is/are a byproduct of degeneration (osteoarthritis) or inflammation (rheumatoid arthritis). If the pathology of the disease is inflammatory, the patient will have elevated blood cytokine levels, along with other biomarkers. One liver-based protein very commonly studied is C-reactive protein (CRP), the biomarker of inflammation studied in this Senior Thesis. It would be elevated, for example in the 10-40 mg/ L range, in the patient with rheumatoid arthritis. It would be normal or near normal in most other diagnosis listed on the differential. Thus, to arrive at a definitive diagnosis for this hypothetical patient, an imaging study and a bloodwork panel that includes cytokine/ inflammatory biomarkers including CRP are needed.

1.2 C-Reactive Protein (CRP)

CRP is a homopentameric (its quaternary structure is composed of five identical polypeptide subunits that are not connected by covalent bonds) plasma protein that is ubiquitous for inflammation and is very commonly ordered as a clinical blood test, as seen above with the hypothetical patient. It was identified in 1930[1] as the third serologic fraction isolated from patients infected with pneumococcus, among those that were already known capsular polysaccharide and nucleoprotein fractions[2].
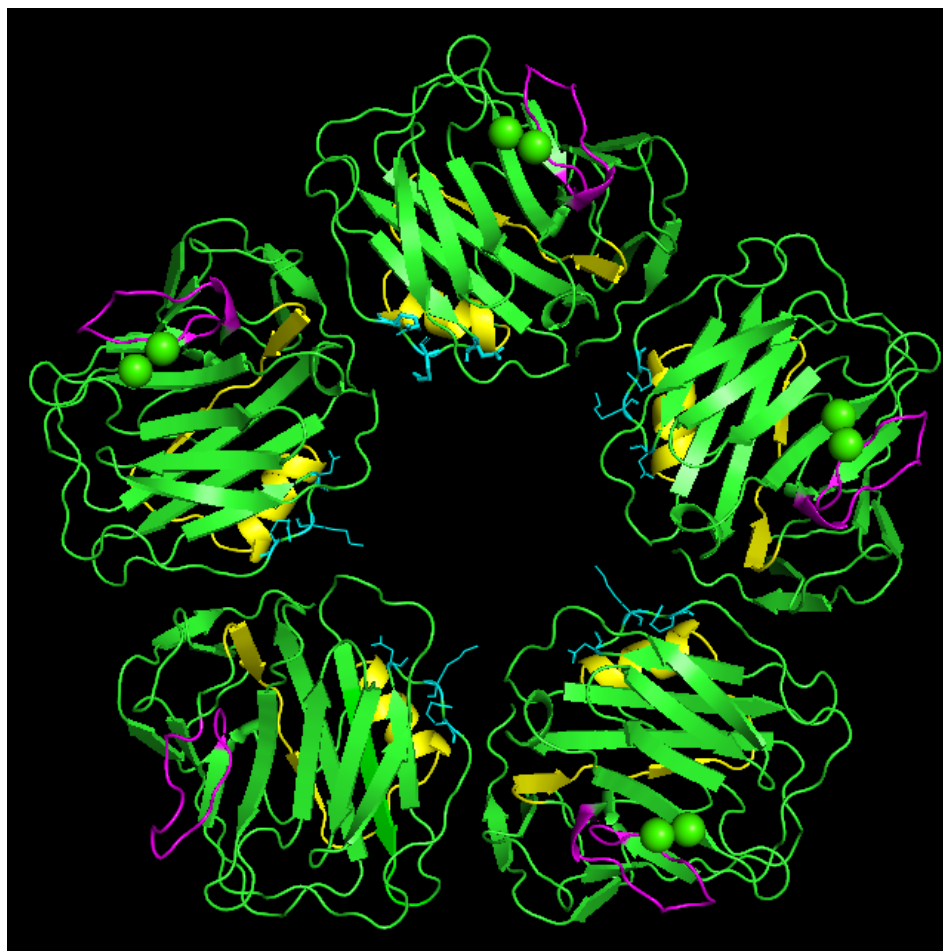
Figure 1.1 – Cartoon schematic of CRP. Residues 134-148 are highlighted purple and residues 152-176 are highlighted yellow. These residues in the primary sequence form the two allosteric calcium binding sites[3]. Asp-112, Lys-114, and Arg-116 are highlighted in cyan and drawn out as lines. These residues bind to C1q when CRP is allosterically activated[4].

Although CRP is used clinically as an inflammatory biomarker, it serves a key role in the innate immune system. CRP is stabilized by two calcium cations per protomer (Figure 1.1). The binding sites for the calcium cations are in close proximity, which significantly alters the tertiary structure of the protomer[5]. This conformational change opens a pocket for phosphocholine, which is widely distributed marker on teichoic acids, capsular carbohydrates, lipopolysaccharides of bacteria, certain

biological membranes, among other microorganisms[5]. This allows CRP to recognize an array of pathogens and damaged host cells needed for phagocytotic elimination[5].

In some cases, CRP can directly opsonize by marking the antigen using IgG Fc-receptors via ligand competition[4]. In other instances, its immune response is much more complex. For example, when phosphocholine binds to the allosteric site in CRP (the recognition step), CRP undergoes a significant conformational change near its central pore, which can then bind complement component 1q (C1q) to Asp-112, Lys-114, and Arg-116 on each promoter (Figure 1.1). C1q is the first protein implicated on the classical complement pathway. C1q is activated upon binding to CRP (in the absence of the complement proteins, the CRP inflammatory responses is largely halted[6]). C1q recognizes an antigen-antibody complex and recruits the entire C1 complex when activated by CRP[6]. This in turn activates C1, C2, and C4 complements to form the C3 convertase, which ultimately leads to a cascade of nine complement proteins to form the Membrane Attack Complex (MAC) on the antigen[6].

Even though many consider the CRP activation of the classical complement pathway as its most important physiological function, it is implicated in so many different immune responses that its complete role in the innate immune system is not fully understood.

However, CRP has emerged clinically as a "go-to" biomarker because of its rapid uptake during an inflammatory event, its ability to exist in very different blood concentrations among different individuals, and its short half-life (18-20 hours). CRP is regulated by various cytokines including IL-6 (primary inducer), IL-1β, TNF-α[6]. Inflammatory cytokines are messenger proteins secreted by various cells in the immune

system to promote inflammation (the primary means of communication between cells of the innate immune system). The cytokines listed above all have the capacity to induce rapidly secretion of CRP that is stored in very high concentrations in the endoplasmic reticulum (ER) of hepatic cells by interfering with the CRP-carboxylesterase bonds, which helps store CRP in the ER[6]. This event can cause CRP levels to rapidly rise in the bloodstream. In fact, with an active infection the levels can increase 1000-fold in 48 hours[6]. For this reason, in medicine, CRP is termed an "acute phase reactant". Additionally, CRP levels decline according to the 18-20 hour half-life when the inflammatory event is resolving and its secretion is no longer promoted. Thus, blood levels of CRP are clinically valuable to monitor acute inflammation as well as its resolution.

One early working use of CRP was its detection in rheumatic heart disease during which cardiac inflammation arises from infection of myocardial cells. Mild inflammation is usually considered to be 10-40 mg/ L, with active bacterial infection causing peak blood concentrations of 40-200 mg / L being consistent with a bacterial infection (e.g. Streptococcal infections that cause rheumatic heart disease). Burns and other severe infections (including severe clinical presentations of human coronavirus infections) will induce higher levels, for example > 200 mg / L.

Additionally, CRP is used for cardiac risk stratification at lower concentrations (0-10 mg/L). While such blood levels are considered "negative" for an acute inflammatory response, there is a cardiovascular literature on "high-sensitivity" (hs) methods for CRP measurement that over time became known as "hsCRP"[7-10]. These rely on reproducible measurements of CRP concentrations of <1 mg / L (low cardiovascular risk), 1–3 mg / L

(moderate cardiovascular risk), and >3 mg/L (high cardiovascular risk). Thus, making accurate, widespread, and inexpensive CRP detection at low levels an interesting potential application of this research.

Clinical labs use particle-enhanced turbidity to determine blood CRP; a typical large urban hospital will run this exam hundreds of times per day on inpatients alone. In clinical CRP measurements using turbidimetry, anti-CRP antibodies are bound to an inert particle such as latex. Turbidimetry refers to correlating the intensity of scattered versus transmitted light to the concentration of suspended particles between the light source and the receptor. Since the concentrations being detected are very low, the test assumes that the suspended particles have negligible solubility. Similarly, the test requires that the particles are sufficiently in solution and have not settled in solution. Immunoturbidimetry refers to the fact that the particles themselves are part of an immune response. In the case of CRP measurements, CRP in blood plasma is conjugated with a commercial anti-CRP antibody. In latex immunoturbidimetry the anti-CRP antibody is bound to latex so that consistent light transmission measurements can be made.

All of the above assumptions are met with a clinical chemistry medical device. There are many examples, one of which is the cobas® line of analyzers by Roche Diagnostics USA[11]; these devices use a mathematical relationship based on Beers' law to read out clinical CRP values. However, even the smallest device in this line – the cobas c111 is a relatively large and expensive device that requires meticulous calibration and care. In internet search on the c111 (that can fit on a desktop) shows a base price of roughly $8,000 USD[11].

1.3 Point of Care (PoC) Testing

Point of Care (PoC) tesing is one method to perform a medical assay; it is generally designed to be relatively inexpensive and does not use trained lab personal to conduct the test. In addition, PoC test kits are deigned to be disposable. Point of care testing is also designed to be conducted rapidly, once the test kit is made available to the consumer (i.e. the patient). Rapid, accurate testing has become paramount in the COVID-19 pandemic. Pragmatic, reliable medical tests to the absolute forefront of public health. This is true in underdeveloped countries such as the pandemic in India (late April, early May 2021) where laboratory equipment is not available.

Medical bloodwork in hospitals and medical centers do not use PoC testing. These tests are routinely run using large medical devices that perform automated functions, for example this is done with immunoturbidimetry. The typical clinical care setting is a well-resourced laboratory with skilled personnel and well-attended, complex medical devices. The ability to conduct many of these experiments comes at the expense of the ability to provide testing, localized testing, or testing at the Point of Care (PoC).

The main limitation of PoC testing is that it can only be practically done for a small fraction of diagnostic medical exams. For example, data that requires blood clot (cells) to be removed from the plasma makes PoC testing more challenging. Tests that require timing a reaction (for example the erythrocyte sedimentation rate), or microscopic inspection (counting of sickled red blood cells) are not amenable for most, current PoC methods. The second limitation is that PoC testing can have higher false

positive and false negative rates than standard laboratory tests. One such example

comes from a 2014 publication from the Whitesides Lab in the Harvard University

Chemistry Department. This work demonstrated electrochemical enzyme-linked

immunosorbent assay (ELISA, discussed in the next section) as a proof of concept to

detect the malarial histidine rich protein from *P. falciparum* (*pf* HRP2), performed

entirely on hydrophobic paper and at a very low cost[12]. Electrochemical ELISA is

typically preformed on microtiter plates using an enzymatic reaction to produce an

electroactive product for quantification. However, the paper device fabricated was at

times ineffective because of false negative (FN) results. The explanation was that the

incubation and washing steps accumulated debris on the electrodes built into the paper

device, which prevented the necessary electron transfer for quantification[12]. Some PoC

false positive (FP) and false negative rates are simply unavoidable. All test

characteristics should be considered in any PoC test; inaccurate rapid PoC tests are

inevitable and therefore in some settings these devices should be considered screening

devices, rather than for a definitive diagnosis.

1.4 ELISA

ELISA is ubiquitous in medical science and in clinical medicine and has become

a staple of PoC testing. This detection assay came to light in the 1970s to study

parasitic diseases; ELISA was originally used in South America to identify individuals

from malaria endemic and non-endemic regions by detecting the *pf* HRP2 antigen on *P.*

falciparum[13], the same antigen that the Whitesides group investigated in 2014. The goal

of any ELISA experiment is to immobilize a specific target antigen onto a solid support

(usually a polystyrene 96 well plate) and to quantify either the antigen or antisera

concentrations using a monoclonal antibody-enzyme complex to perform the readout

using a known enzymatic reaction.

Antigen immobilization is at the heart of standard ELISA experiments (reverse

ELISA uses a slightly different procedure). The dynamic interplay between the protein

absorbed onto the solid support and the aqueous layers that encounter the solid support

is crucial for any ELISA assays (Figure 1.2). Antigens can either be directly immobilized

or indirectly immobilized.
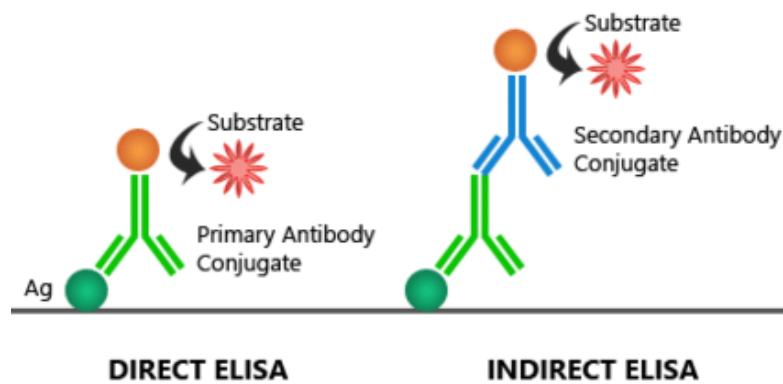
Figure 1.2 – Schematic of Direct vs. Indirect ELISA[14].

The first step of a direct ELISA experiments is to immobilize the antigen onto the

solid support. Direct ELISA experiments typically quantify the presence (or lack thereof)

of antibodies in a patient's blood serum and are considered antisera tests. One very

important and extensively studied antisera direct ELISA experiments is the COVID-19

IgG antibody test. In this ELISA test, the receptor binding domain (RBD) of the COVID-

19 spike (S) protein is immobilized onto a 96-well microtiter plate[15]. The patient's blood

serum is then added to the microtiter plate; if the patient has SARS-CoV-2 IgG

antibodies (meaning the patient has potential immunity from a prior viral infection and/or a vaccine), these antibodies will bind to the microtiter plate coated in S-protein RBD and will remain immobilized after washing steps[15]. A secondary anti-human IgG antibody labeled with horse radish peroxidase (HRP) is added and binds to the Fc domain of any of the patients immobilized SARS-CoV-2 IgG antibody from his or her blood serum[15]. Any unbound anti-human IgG-HRP will be washed during the washing step. The HRP substrate (o-phenylenediamine dihydrochloride) is then added, and the visual formation of yellow indicates a the presence of SARS-Cov-2 IgG antibodies (qualitative) optical density at 490 nm is monitored to quantify the concentration of SARS-CoV-2 IgG antibodies (quantitative)[15].

In indirect, or sandwich ELISA, the capture antibody must first be adsorbed to the solid phase. Thus, this experiment directly measures for the presence of antigens in a sample. One of the most commonly used ELISA experiments in the clinical setting, ABO blood typing, uses indirect ELISA. In ABO blood typing, monoclonal antibodies for blood antigen A (anti-A mAbs) and monoclonal antibodies for blood antigen B (anti-B mAbs) are first immobilized onto different polystyrene wells of the 96-well microtiter plate and washed to remove excess capture antibodies[16]. The patient's blood sample is then diluted in buffer and added directly onto both the anti-A mAbs well and the anti-B mAbs well. If either antigen is present on the surface of the patient's red blood cells (RBCs), the RBC will be tethered to the capture antibody. The detection antibody (anti-A/B mAbs-HRP) is added to the appropriate well and any unbound detection antibody will be removed during the washing step. Both the ABO blood staining experiment described by Kimura, et al. and the COVID-19 IgG antibody test use an identical enzymatic assay;

the visual formation of yellow indicates the presence of the blood antigen A or B on the

surface of the patient's RBCs (qualitative). The Methods in this project use an indirect

ELISA to detect the antigen CRP in blood serum. The enzyme in the indirect CRP

ELISA is alkaline phosphatase (ALP), which uses a 5-bromo-4-chloro-3-indolyl

phosphate/p-nitroblue tetrazolium chloride (BCIP/NBT) as its substrate (Figure 1.3).

ALP hydrolyzes BCIP to form an intermediate, which reacts with NBT[17]. In the reaction,

NBT is reduced to NBT-formazan, while the BCIP intermediate dimerizes to form 5,5'-

dibromo-4,4'-dichloro-indigo white[17]. This product is an indigo dye that can measured

calorimetrically.
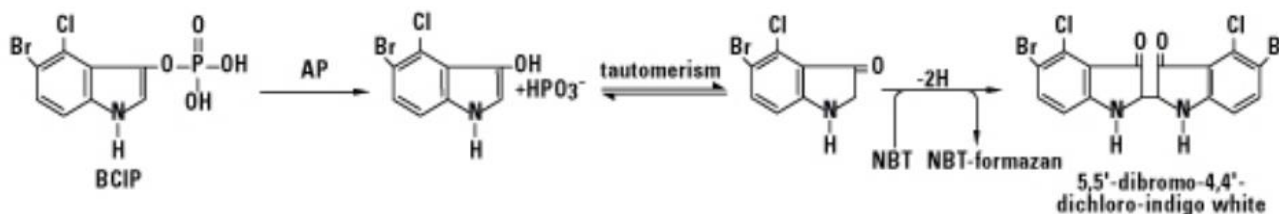
Figure 1.3 – Enzymatic Readout for ALP conjugated antibodies using a BCIP/NBT
Substrate[17].

1.5 Microfluidics, or "Lab on a Chip"

The term microfluidics refers to movement and analysis of a "micro" (10^{-6} – 10^{-18}

L) volumes of fluid. In addition to the inherent capillary action, fluid movement can be

enhanced by several mechanisms. The general system includes making groves/ wells

on the surface of a chip[18]. These channels enhance motion and the interaction between

macromolecules, thereby allowing a readout on a second layer or film, known as a "Lab

on a chip". Such "labs" can be quite intricate, sophisticated, and expensive to construct

because fluidic channels need to be so small and precise that the solution flow changes from turbulent to laminar flow. Consequently, these systems are not yet routinely used in day-to-day medical care – however, they are increasingly used for medical research. As an example of the complexity of some of these microdevices, cardiac microtissues can be engineered in multiple layers, using pressures as well as fluid flow to study the response of human pluripotent stem cells to different drug exposures[19].

Microdevices are composed of three main parts: the analytes being quantified, the type of microdevice platform, and the detection assays. Analyte readout is at the heart of all laboratory/PoC-based diagnostics. These systems are designed to analyze samples by quantifying certain analyte concentrations within the sample. Analyte readout requires three simple, but essential elements: targeting a specific analyte, recognizing the element, and transducing a signal[20].

In microfluidics, high affinity monoclonal antibodies for a specific antigen are commonly immobilized onto a solid phase within the microfluidic device. Immobilization is a technique used to provide a rigid link between a solid support (such as PDMS, PMMA, PS, glass beads, magnetic beads, paper, metallic nanoparticles, silicon, etc.) and a biomolecule, such as a capture antibody[20]. In some cases, the solid phase must be covalently modified before immobilization can occur. For example, Zhang, et. al. described the adsorption of albumin, fibrinogen, and IgG to a polyethlene glycol (PEG) immobilized silicon surface[21]. PEG chains are very long macromolecules commonly used in immobilization steps because of their ability adsorb a variety of proteins and stabilize them in the solid phase.

Immobilization assays have advantages and disadvantages relative to standard solution-based assays. Multipoint and multisubunit attachments to proteins provide rigidity and stability to the protein[22]. Proteins in aqueous solutions are incredibly dynamic structures that can easily denature. Protein stability is heavily influenced by temperature, pH, solvent, presence of surfactants, etc[22]. Accordingly, aqueous proteins are highly thermo-sensitive. However, the multipoint attachments on the solid phase hold proteins firmly in place, making denaturation much more difficult. Other advantages to immobilization assays include an improved process control, less labor intensive assay, more cost effectiveness, better safety profile, and more environmentally friendly[22]. However, there are some challenges to solid support immobilization, which include lower enzymatic activity/ capturability of an antigen, the possibility of protein denaturation, mass transfer limitations, the possibility that the immobilization technique blocks the active site of the protein, and conformational changes in the protein during the immobilization step that render it inactive[22].

The key concept behind immobilization is that some protein will be lost/inactivated during the immobilization step. However, the fraction of protein properly immobilized onto the solid support is highly stable and ready to use when the device is needed. This is essential because many PoC devices need highly stable proteins to carry out certain reactions to rapidly transduce a readable signal. These devices would be highly ineffective if they needed the special solution conditions only found in a lab-based setting (i.e. many aqueous antibodies/enzymes need to be stored in highly specified buffers at a particular pH at -80°C). Thus, any immobilization assay is only successful if the molecule of interest is immobilized in a near-quantitative fashion, has

long term stability, can interact with the mobile solution phase, and does not interfere with the detection assay[23].

The limit of detection versus sample size is at the heart of microfluidics. Smaller scales translate to a low absolute number of antigens. Typically, this means that sensitivity of the test would depend on the concentration of antigen in the sample being tested. However, in some cases, the limit of detection can increase on a microplatform. Diagnosing malaria (different from the original malaria ELISA conducted in the 1970s, described above) is an interesting example of how microfluidics could be integrated into clinical care. Currently, patients are diagnosed via application of a Giemsa stain whole blood, after which the stained parasite can be seen with a standard microscope. While commonly used, there are limitations to this technique. One advantage of microfluidic detection is very small volume needed e.g. the detection of blood malarial parasites can be achieved with samples of 21.3 ± 2.1 μL[24]. Moreover, there is increased species identification with detection of 80-200 parasites μL^{-1} with 90% accuracy[24]. Thick blood smears not only require a larger sample, but also the morphology of the parasites can be obscured. Moreover, conventional malaria testing cannot be integrated into a compact packaging flow as is the case for a microfluidic lab on a chip.

1.6 Paper Microfluidics: Paper Chemistry and Fabrication Techniques

As suggested in the Microfluidics section above, there is considerable research on the design of complex labs on a chip using a variety of solid phases. Microfluidic paper-based analytical devices (μPADs) offer an attractive alternative to some of the complicated and expensive microfluidic platforms because μPADs are simpler, less

expensive, and potentially more usable in resource limited settings[25]. Accordingly, these devices have broad applications in PoC testing, public health, food quality control, and environmental monitoring[25].

Paper has a quite unique solid phase with many versatile applications for microfluidics. The interstitial space in a paper matrix creates tiny chemical reaction zones that can hold reactants in place and push products through the paper device using capillary action[24-26]. Thus, the interstitial spaces in paper act as microenvironments that can be tailored to mimic native cellular environments. Accordingly, paper has become an attractive alternative to analyzing cell cultures relative to the conventional method that uses well plates[25].

One key advantage that paper devices hold over all others with solid phases is the ability to easily and readily fabricate hydrophobic barriers onto the solid phase. Other solid phases require meitculous etching/fabrication of extrememly high resolution micrscopic channels in the solid support. Hydrophobic barriers that create leak proof sections in the paper to geometrically manipulte the aqueous layer into the deisred orientation[26] can be readily added to paper substrates using both chemical and physical methods. Common chemical methods of μPAD device fabrication include photolithography (a photoresistive liquid hardens when exposed to light[25]), plasma treatment (a hollow metal mask can be used to genertate hydrophilic channels in a preteated hydrobphobic sheet of paper[25]), and inkjet printing (toluene is printed on paper coated in polystrene in a single step to create microfluidic channels). Common physical methods of μPAD device fabrication include printing (such as screenprinting), stamping, drawing/plotting, spraying, and dipping[26]. Physical pore-blocking methods are

cleaner and cheaper because the number of production steps are limited and the paper is only treated where hydrophobic barriers are required[26].

Another novel component of µPADs involves the configuration of the device. Paper, being so versatile, has the ability to be aranged in many different fashions. The simpliest devices are termed "lateral flow sensors" or two-dimensional (2D) µPADs. These devices have a unique hydrophobic pattern that controls fluid flow on a singular piece of paper. Thus, capillary action only occurs in the plane of the paper and the solution is only allowed to flow "laterally". Three-dimensional (3D) µPADs on the other hand have "vertical flow". In these configurations, multiple layers of paper are stacked on top of one another and hydrpobic barriers from succesive layers are connected to generate a fluidic path that penetrates the device. Paper is an attractive scaffold for 3D designs because of its thickness, pore size, rigidity, flexibility, chemical composition, and surface properties[25]. The main advantage of a 3D device is that a single inlet can create fluidic paths to multiple detection zones because of the vertical and lateral manipulation of the hydrophobic barriers[25]. However, one large limitation to both 2D and 3D µPADs is that the singular fluidic channel limits the complexity of the assay. Any complex assay that requires a timely mixing of multiple reagents followed by washing steps, such as enzyme-linked immunosorbent assay (ELISA), cannot be conducted in a singular fluidic channel. A critical index paper for this Senior Thesis bypassed this limitation of paper microfluidics by engineering a sliding strip, also known as a "SlipChip". The sliding strip allows the device to switch fluidic paths during the assay; as the chip is pulled out of the device (at fixed intervals denoted by lines on the sliding strip), different fluidic channels are connected to the test zone, thereby enabling a

multistep complex assay on a paper device[27]. The physical movement of the test zone is responsible for connecting the fluidic paths.

The initial methods in this project proposed to use a "SlipChip" design to quantify CRP blood concentrations. The rationale for attempting to reproduce this 2018 paper-based ELISA is that the conventional 96-well ELISA requires well-trained personnel, expensive instruments, and multiple mixing and washing steps. As detailed in the Discussion (Limitations), these methods were technically not feasible, after which the current methodology was proposed.

Not all paper substrates are identical, and chosing the proper paper subrate is an important part of running any paper based test. The two most common paper substrates used in the fabrication of µPADs are polyvinylidene fluoride (PVDF) and nitrocellulose (NC) nitrocellulose[23, 25]. These substrates are validated for ELISPOT (Enzyme-linked immunospot) assays[25]. PVDF has received considerable attention in biotechnology and bioseparation applications because PVDF membranes possess strong mechanical properties, have high hydrophobicity, and remain chemically inert to many solvents. Its strong hydrophocity and durability make it the ideal paper substrate for northern, southern, and dot blots, as well as amino acid analysis and protein sequencing for very small quantities of protein[28]. Moreover, these membranes can be heat sterilised without change of the membrane porosity.
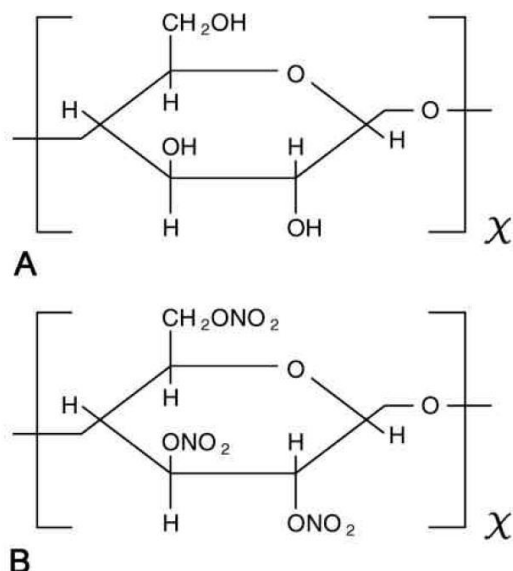
Figure 1.4 – The structure for the monomer unit for cellulose (A) and NC (B)[23].

NC, a derivative of cellulose that replaces hydroxyl group with nitrates (Figure 1.4), is a very brittle paper subsrate that is widely used in immobilization assays that involve proteins, glycoproteins, and/or nucleic acids[23, 28]. The key element that makes NC such an attractive paper substrate is its micro pores (0.5-10 micrometers)[23]. The micro pores act as small traps that physically capture macromolecules. While the exact chemical mechanism that holds immobilized biomolecules in place is unknown, a wide of array of noncovalent and hydrophobic interactions are partly responsible for immobilization[23]. Drying and/or baking is needed to complete the immobilization step[23]. One drawback of NC membranes is that they are not optimal for electrophoretic transfer of nucleic acids due to the high salt concentrations present in these experiments[28].

1.7 Paper microfluidics: assays

Not only is the paper itself highly versatile, but also the chemical assays can be highly varied. The readout of µPADs can be designed using colorimetric[27], flourescent[24],

chemiluminescent, and electrochemcial assays[12]. The three colormetric assays

described in the ELISA section (COVID-19 IgG antibody test, ABO blood typing, and the

CRP index paper for this Senior Thesis) all use colorimetric ELISA assays. Colorimetric

assays are the most common rapid PoC assays because results can be quickly

analyzed (e.g. qualitatively).

Even though only ELISA-based colorimetric PoC assays have only been

introduced to date, it is important to note that most colorimetric PoC assays used in the

clinical setting are not ELISA-based. Rather, most PoC colorimetric use Gold

immunochromatographic assay (GICA) test strips (in some cases a blue-colored latex is

used in place of gold nanoparticles). These devices are often preferred in a resource

limited setting because they are self contained (ELISA needs external reagents). GICA

use a simple lateral flow test with all needed reagents stored inside the device. Two

important GICA test strips are the home pregnancy test and the BinnaxNOW COVID-19
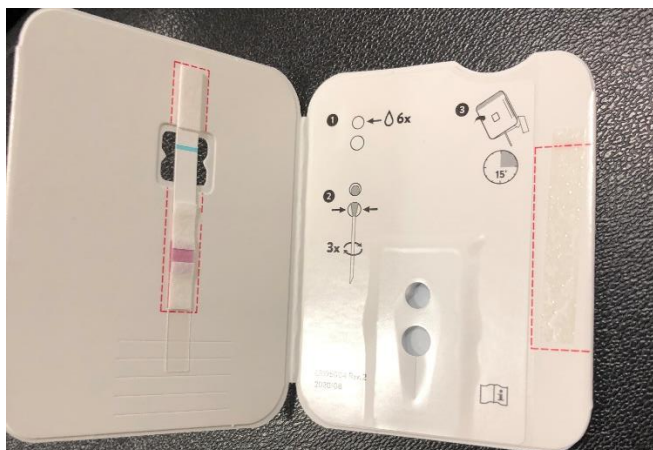
Rapid test.

A.
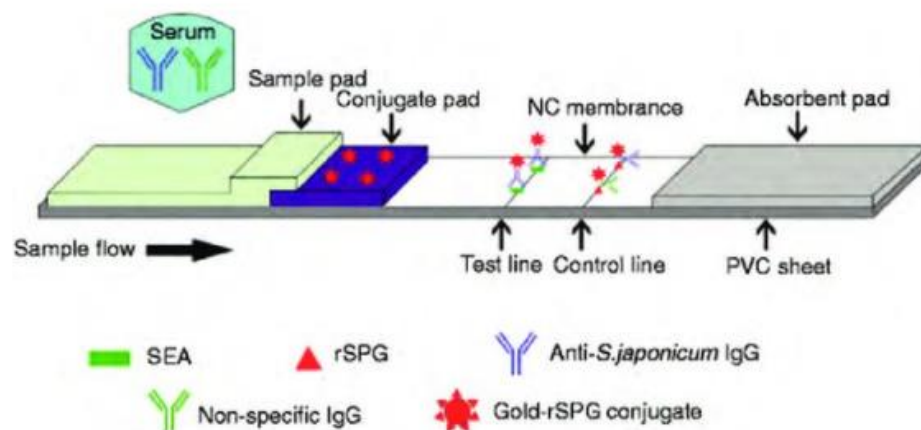
B.

Figure 1.5- A. GICA schematic[29]. B. BinnaxNOW COVID-19 rapid kit provided to Bard student-athletes as a screening tool before intercollegiate games can proceed.

Both of these GICA tests are designed to detect the presence of an antigen in the sample: human chorionic gonadotropin (hCG), a protein that is only produced in developing placenta is the target in the home pregnancy test and the spike protein on the novel coronavirus is the target fot the BinnaxNOW COVID-19 Rapid test. When each sample is added to the sample pad, simple diffusion of a working solvent (the urine in a pregnancy test and the working buffer provided with the BinnaxNOW COVID-19 Rapid test kit) intiates the assay.

As the sample moves from the sample pad to the conjugate pad, it encounters highly specialized capture antibodies (that target the antigen of interest) that have been conjugated to gold nanoparticles (AuNP)[29]. The AuNP-antibody conjugate is freeze dried into the conjugate pad to perserve stability of the capture antibodies[29]. These AuNP-antibody conjugates are eventually mobilized in the working buffer and are driven onto the nitrocellulose test strip using capillary forces[25]. This test strip has two bands of immobilized capture antibodies: the test line has antibodies that recognize a different

epitope on the antigen of interest and the control line has antibodies that recognizes the conserved domain of the conjugated AuNP-antibodies[29]. Thus, if the desired antigen is present in the sample, the test zone will form an antibody-antigen-antibody-AuNP sandwich. The control line antibodies will bind excess unbound AuNP-conjugated antibodies. The AuNPs form a red band when they are immobilized in close proximity, making the readout direct and rapid (~ 5 minutes)[25, 29]. Thus, a positive home preganancy/ rapid COVID-19 test contains a red band at both the test zone (antibody-antigen-antibody-AuNP detected) and the control zone (Au-NP-antobody conjugates are functional and have not denatured). A negative test contains one red band at the control zone (the antigen sandwich was not detected at the test zone, but the AuNP-antibody conjugates were still considered functional) and an inconclusive test fails to produce a band at the contol line (the AuNP-antibody conjugates are nonfunctional and have likely denatured).

Both fluorescent-based and chemilumescent-based µPAD assays are similar to colorimetric assays in that the signal being quantified is a color and its intensity is proportional to the concentration of antigen in the sample. Additionally, both assays are more precise than a colorimetrical assay because both assay techniques use instrumentation to quantify the color readout, whereas colorimetric assays can be influenced by ambient light intensity and individual mood/eye conditions (qualitative "yes or no" human analysis)[25]. In both chemiluminescent and fluorescent assays, light is emitted after particle excitation. Chemilumiscence uses an enzymatic reaction that generates an unstable intermediate that emits a photon during relaxation and fluorescence uses a fluorophore that is excited by a high energy light source that emits

a photon upon radiative relaxation. Since both assays require an advanced imaging source to conduct a readout, they have fewer applications at the PoC level.

Challenges notwithstanding, a fluorescent paper-based lab on a chip to diagnose malaria was described above. Horning et al. devised a paper cartridge that delivers a remarkably small blood volume stained with acridine orange (AO) to an optically transparent chamber suitable for microscopy[24]. The capillary action of the cellulose matrix delivers the blood stain to the microscopy chamber in the paper device[24]. The AO dye differentially stains DNA and RNA, allowing the morphological features of the nucleus/cytoplasm of malarial parasites to be visualized under a microscope[24]. A "positive" malarial test is when AO dye stains malarial parasites that are visualized fluorescently under a microscope.

Additionally, an electrochemical paper-based assay from the Whitesides Lab was described above. Coincidentally, this µPAD is also designed to quantify malarial parasites. However, in this experiment, a sandwich ELISA assay was used to quantify the malarial histidine rich protein *plasmodium falciparum* (*pf* HRP2). A capture antibody was adhered to the graphite ink embossed well that recognizes and binds to the *pf* HRP2 antigen[12]. A detection antibody conjugated to ALP was then eluted over the embossed well and only adhered to the well if the antigen was captured from the sample. The Whitesides group used a different ALP substrate, p-nitrophenyl phosphate, which is hydrolyzed to 4-amino phenol (pAP)[12]. pAP can be quantified both colorimetrically (a yellow color is produced and absorbance at 405nm can be taken) or electrochemically (pAP is a reducing agent that produces an electrochemical signal that can be measured using square-wave voltammetry, SWV)[12]. After the enzymatic reaction

was allowed to occur for 10 minutes, SWV was conducted by generating an pulsating

electrochemical potential between the electrodes embossed on the paper device and

relating the peak current to pf HRP2 concentration[12].

These unique and very different paper-based assays highlight the countless

potential applications of paper devices. This field of research is exciting with ample

opportunities for future development.

1.8 COVID-19 and the Impact of Testing

COVID-19 has brought the timing and accuracy of medical testing to the

international limelight. There are two general classes of test, those that can be

performed rapidly and at the PoC, and those that depend on Polymerase Chain

Reaction (PCR) and are performed in hospital medical centers/labs.

Reverse Transcriptase (RT)-PCR is considered the reference standard for rapid,

PoC COVID testing. RT-PCR directly detects viral RNA with high sensitivity and

specificity. During the time of writing this Project (mid-April 2021), the US FDA provided

Emergency Use Authorization (EUA) for home, self-testing without the need to ship

samples to a lab. The EUA also removed the need for a prescription from a healthcare

provider. This important, dramatic move has changed healthcare in the United States.

The test available from the CVS pharmacy chain is made by Abbott and as noted

above, has the commercial name BinaxNOW™ COVID-19 Antigen Self-Test. It is

marketed and sold as "a simple solution for COVID-19 infection detection, with rapid

results in the convenience of your home" on the CVS website. The equivalent Abbott

test outside the United States is the Panbio™ COVID-19 Ag Rapid Test Device (Abbott

Diagnostic GmbH, Jena, German). The chemistry and mechanism behind this GICA

assays in both COVID-19 rapid antigen tests is described above. The key clinical

relevance of these devices lies in quality control.

All tests, especially those at the PoC level, must have meticulous evaluation of

the FN and FP rates. The COVID-19 pandemic has demonstrated the immense need

for rapid and accurate screening tools and its implications on community spread/quality

of life. The impact of FN and FP rates was briefly mentioned in an earlier section, when

discussing the fouling of electrodes on the electrochemical μPAD designed by the

Whitesides Lab. However, the impact on COVID-19 and current public healthcare

warrants specific analyses

For FDA clearance under EUA, the COVID-19 rapid tests were considered with

respect to reverse-transcriptase polymerase chain reaction (RT-PCR) as a reference

standard. Over the past year, many different research groups have published the test

characteristics for the GICA-based rapid antigen assays for COVID-19. The sensitivity

and specificity data are extremely important factors for global public health. Fenollar

etal. published a clinical trial on the Panbio™ COVID-19 Ag Rapid Test Device[30]. This

clinical trial consisted of 341 patients (182 symptomatic patients and 159 asymptomatic

patients deemed "close contacts")[30]. All 182 symptomatic patents were RT-PCR

positive. However, only 144/182 were true positives (sensitivity 79.1%) and 38/144 were

false negatives (20.9% false negative rate) using the Panbio™ COVID-19 Ag rapid test

device[30]. Of the 159 asymptomatic patients, 22 were RT-PCR positive and 137 were

RT-PCR Negative. Of the 22 RT-PCR positives, 10/22 were true positives (sensitivity

45.4%) and 12/22 were false negatives (54.5% false negative rate)[30]. Of the 137 PCR

negatives, 130/137 were true negatives (specificity 94.9%) and 7/137 were false

positives (5.1%)[30]. Despite being a relatively small sample size, these results are consequential. A 79.1% sensitivity among symptomatic patients and a 45.4% sensitivity among asymptomatic patients indicates that these tests are ineffective at minimizing communal spread; patients who test negative will assume they cannot transmit the virus due to their test, but in reality, may contribute to enhanced viral spread because they are not required to shelter in place. The clinical impact of this early work was that the low false positive rate (5.1%); this suggests that a positive rapid test should be considered almost a definitive diagnosis.

A second paper reported another clinical trial for the Panbio™ COVID-19 Ag Rapid Test Device[31]. This clinical trial consisted of 958 patients[31]. This paper did not specify groups of patients being tested because of active symptoms or a suspected exposure. 359 patients were RT-PCR positive and 599 patients were RT-PCR negative[31]. Of the 359 RT-PCR positives, 325/359 were true positives (sensitivity 90.5%) and 34/359 were false negatives (9.5% false negative rate)[31]. Of the 599 PCR negatives, 592/599 were true negatives (specificity 98.8%) and 7/599 were false positives (1.2%)[31]. These results were far superior to those in the smaller study, further suggesting that the Panbio™ COVID-19 Ag Rapid Test Device is powerful screening tool.

Analyses of these two important publications prompted the investigation of similar test characteristics for this Senior Thesis, using those data and methods available in the scope of the experiments.

2. METHODS

2.1 Rationale: Decision to Use Screen-Printing in lieu of Wax Printing

The µPAD design, µPAD fabrication, and assay procedure closely followed the index paper by the Whitesides Lab[27]. However, the µPAD fabrication for this thesis could not completely mimic their design because Bard College does not have a wax printer. The Whitesides Lab used a wax printer to directly print hydrophobic patterns onto Whatman No. 1 chromatography paper and Nitrocellulose membranes[27]. The wax was then melted into the paper substrates (a heat gun was used to melt the wax into the chromatography paper and a oven preset to 140°C was used to melt the wax into the nitrocellulose membrane)[27]. As a work around, this thesis used a screen-printing apparatus to fabricate the hydrophobic barriers in the paper.

The screen-printing concept was adapted from Sitanurak, et. al[26]. In this paper, the authors describe a proof-of-concept µPAD design for both a 2D and a 3D apparatus using screen-printed hydrophobic barriers that have similar sensitivities to paper devices made with standard wax barriers, paper devices that have undergone plasma treatment, and PDMS devices[26]. Screen-printing is a process that uses a negative stencil on top of a mesh platform that allows ink to be pushed onto a paper substrate as the positive image (Figure 2.1).
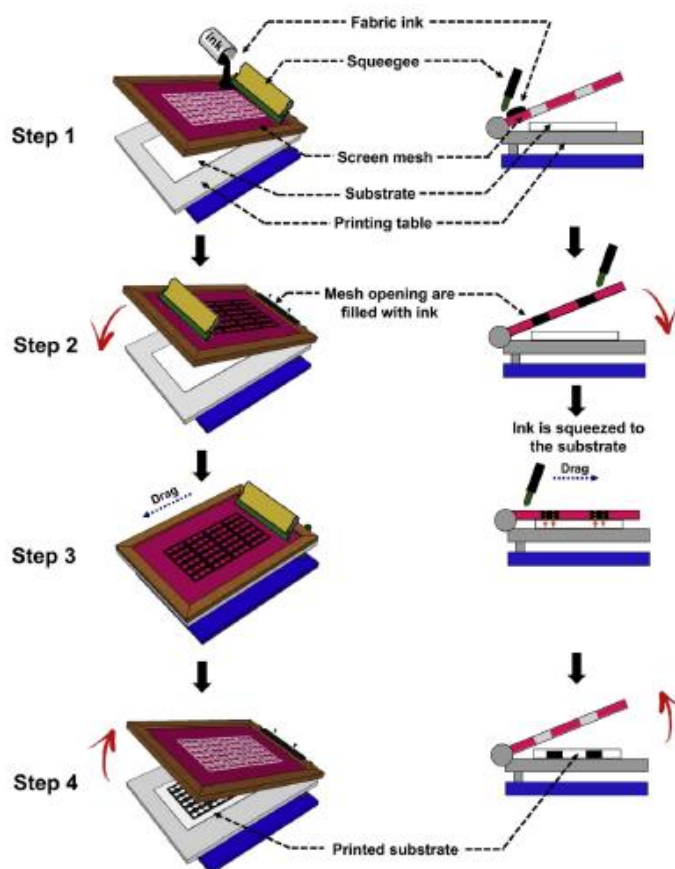
Figure 2.1 – A generalized screen-printing procedure[26].

Sitanurak, et. al. optimized the screen-printing procedure above using PVC (polyvinyl chloride) ink purchased at a local screen-printing store in Bangkok on Whatman grade 4 chromatography paper[26]. The PVC ink was mixed with an organic solvent reducer (optimized at 35 parts PVC ink to 65 parts ink reducer)[26]. After the printing step (Figure 2.1) paper substrates were not cured; they were dried for 15 minutes under ambient condtions[26]. The hydrophobicity of their dumbbell-shaped pattern was probed qualitatively; an optical microscope was used to determine leakage of the hydrophobic barrier (Figure 2.2).
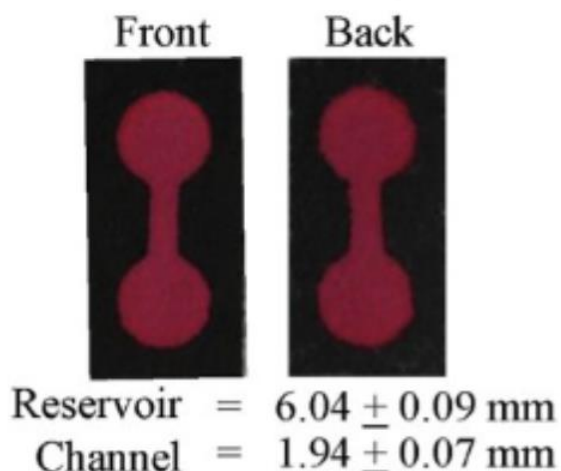
Figure 2.2 – One screen-printed pattern from Sitanurak, et. al. retaining very high hydrophobic resolution on both sides of the chromatography paper[26].

This thesis attempted to mimic this proof-of-concept experiment but was unsuccessful in doing so. This is further detailed in the Limitations section of the discussion.

Additionally, there is a major inconsistency in the proof-of concept experiment that does not make sense for a PVC ink-based print. The authors write "the printed material is taken out and hung to dry at ambient temperature in a good ventilation environment. Usually the substrate is dry within 15 minutes"[26] At this point, the authors declare the paper devices ready for testing. However, PVC inks are thermosensitive; all PVC inks require a high temperature curing step to polymerize the plastic resins[32]. This inconsistency reported by Sitanurak, et. al. raises concern regarding the reliability of the data (PVC ink was either incorrectly reported or the procedure is incorrect).

Another potential reason the proof-of-concept experiment failed is that the wrong chromatography paper was used. Sitanurak, et. al. reported that Whatman grade 4 chromatography paper was the best paper substrate for screen printing[26]. However, this thesis uses Whatman grade 1 chromatography paper, in accordance with the

Whitesides lab[27]. Even though Whatman grade 4 chromatography was the optimized

selection in the proof-of-concept experiment, Whatman grade 1 chromatography was

successfully screen-printed on as well[26].

2.2 Screen-Printing using a Photolithographic Plate

There are three basic techniques used to generate a negative image onto a

mesh screen: a cut paper stencil, drawing fluid/screen filler, and photoemulsion[33]. The

first two techniques are simple. When a negative stencil is put on top of the screen, the

positive image will be pushed through the mesh onto the substrate[33]. Even though

Sitanurak, et. al. do not specify how they created their screens for screen printing, their

procedural schematic (Figure 2.1) appears to be a paper stencil. The drawing method

uses a dissolvable drawing fluid that is drawn onto the screen (positive image). Then

the screen is coated with a screen-filling ink. The screen-filling ink is blocked where

drawing ink is located on the screen. Thus, when the screen is rinsed under a sink, the

drawing fluid is dissolved and the screen-filling ink compromises the negative image of

interest[33].

The final technique, photoemulsion, is the most complicated, but is also the most

precise. Photoemulsion is the technique used in this thesis. Despite being much more

complicated than the other two techniques, its application is very similar to that of the

drawing fluid/screen printing technique.

Screen printing using photoemulsion is a type of photolithography.

Photolithography uses a liquid photoresist, such as SU-8, that solidifies under exposure

of a light source to directly create highly specified patterns[25]. The photosensitive

aqueous layer contains two essential components: a light sensitive polymeric compound

and a lipophilic polymeric compound[34]. These compounds are mixed and dried on a mesh screen in a dark room at room temperature[33]. After the drying step is finished, the positive image of interest is placed directly onto the mesh screen and the image is developed by a high-powered light source. For this experiment, the positive images (Appendices A-E) were printed on an inkjet transparency and fastened to the mesh using a glass slide (designed to push the transparent ink directly against the dried photoresistant liquid to maximize resolution). After the screen was washed, only the negative stencil remained. This is a common application of simple photolithograpy[26, 33-36]. The generated negative stencil allows printing ink to pass through the mesh template[26, 33].

The Speedball Advanced All-In-One Screen-Printing Kit uses a cheap photosensitive aqueous layer. In the Speedball Diazo Kit, a high molecular weight diazo compound, which is denoted the "Sensitizer", is added to polyvinyl alcohol (PVA), which is denoted the "Photo Emulsion Liquid"[33].

Large macromolecules with diazo groups are highly amenable for photolithography because the diazo functional group is thermally unstable, exceptionally light sensitive, and readily forms carbene intermediates[37]. These carbenes readily undergo different insertion reactions under exposure to light[37], especially with the hydroxyl groups studded along the PVA photoemulsion liquid. The carbene insertion reactions form ether bridges with the PVA at these hydroxyl groups. Consequently, the PVA hydrocarbon backbone blankets the diazo molecule with the hydrocarbon backbone of PVA, which hardens to form the stencil[36] (Figure 2.3 C).

A.
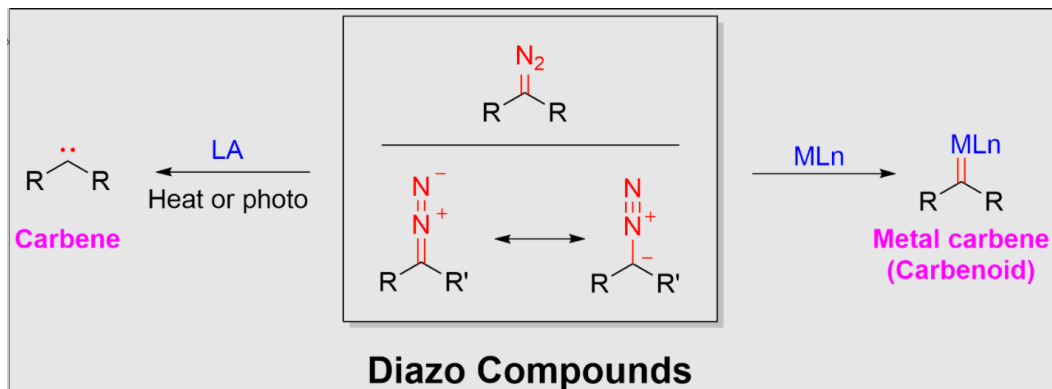
Diazo Compounds

B.
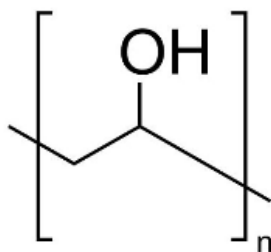
C.
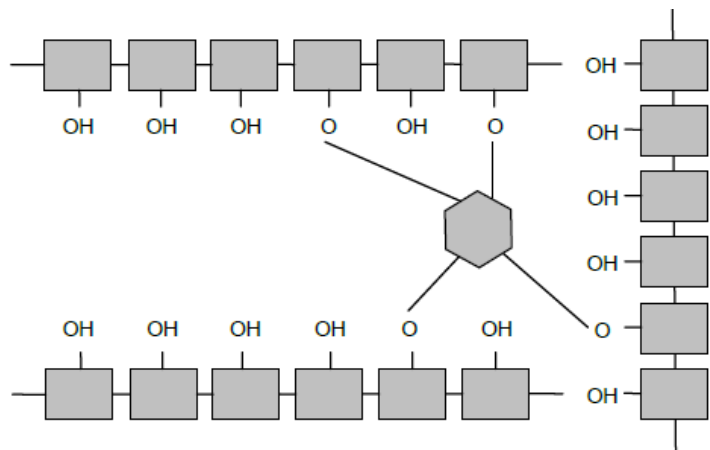
Figure 2.3 – Illustration of photoemulsion screen-printing chemistry. A. Chemistry of Diazo Compounds[38]. B. Structure of PVA[39]. C. This schematic outlines the mechanism by which the diazo polymer (represented by the grey hexagon) forms ether linkages with PVA (the hydrocarbon backbone is represented by grey rectangles)[36].

The screen-printing procedure for the Speedball photoemulsion kit made by Dan Ibarra was followed exactly to fabricate the designs in Appendices A-E. Rapid Cure

Plastisol Ink Black (Screen Print Direct) was mixed with Plastisol Ink Reducer/Detackifer

(Victory Screen Printing) in approximately a 35:65 ratio, as described by Sitanurak, et.

al.[26]. The layers were added together using the paper-tape-paper sandwich described

by Verma, et. al.[27]. The tape was carved using an exacto-knife, but had the device

permitted fluidic flow, a laser cut file (Appendix F) and 3D tape alignment designs

(Appendix G) where ready to be implemented, as was done in the Whitesides Lab.
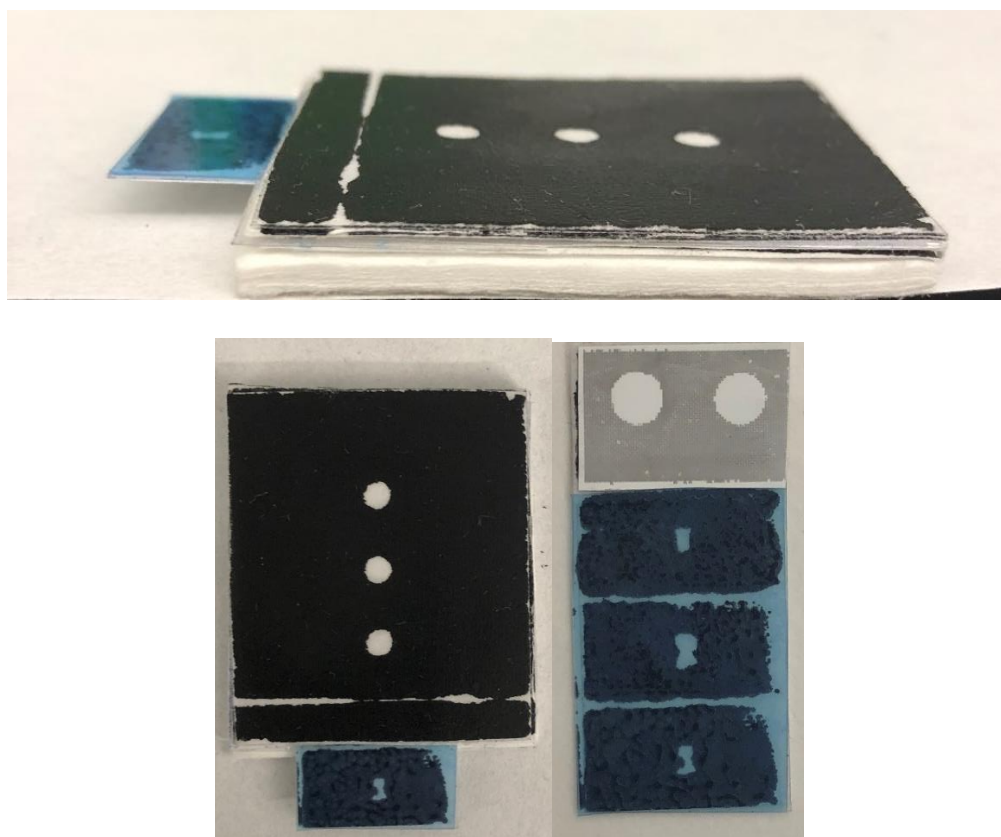
Figure 2.4 – Failed µPAD made using the schematic generated by the Whitesides Lab. Top: Side view of device. Bottom left: Top view of the device. Bottom right: Sliding Strip (NC membrane tape to the strip. The strip is coated in PET film to facilitate the device operation by reducing friction when pulling the sliding strip out).

Since µPAD fabrication failed, the experiments turned to a CRP ELISA

immunodot assay. This point marked a major methodology change. A immunodot (or

ELISA-dot) is a immunological test where a minute amount antigen/antibody is dotted onto a NC membrane and the enzyme readout quantifies a chromogenic substrate[40]. Since many of the assay readout for both the immunodot and the µPAD are the same, most of the materials and procedure initially developed from the index paper[27] could be used.

2.3 Materials

Nitrocellulose membrane, 0.45 µm (Catalog Number 620116) and extra thick (2.45 mm) blotting filter paper (Catalog Number 1703969) were purchased from Bio-Rad Laboratories (Los Angeles, CA, USA). R&D CRP ELISA kit (Catalog Number DY1707), Recombinant human CRP (Catalog Number 1707CR200), and TweenTM 20 (Catalog Number AAJ20605AP) were purchased from Fisher Scientific (Boston, MA, USA). The R&D CRP ELISA kit contains anti-human C-reactive protein (CRP) capture antibodies and biotinylated anti-human CRP detection antibodies. Streptavidin-alkaline phosphatase (ALP) was purchased from Thermofisher Scientific (Waltham, MA, USA). 5-bromo-4-chloro-3-indolyl phosphate (BCIP)/nitro blue tetrazolium (NBT) tablets were purchased from Sigma-Aldrich (Atlanta, GA, USA). The Speedball Advanced All-In-One Screen-Printing Kit was purchased from Amazon. Solid BSA and 10X PBS stock solutions were gathered from Professor Jain's Lab. DI water was used for buffer dilutions.

2.4 Procedures

Test Zone Fabrication:

The sensing dock (Appendix E) was screen printed onto the NC membrane using the protocol written by Dan Ibarra[33]. A plastisol ink/reducer solvent (ratio 35 parts plastisol ink to 65 parts reducer) was pushed through the screen onto the nitrocellulose membrane. The plastisol ink was cured in the drying rack of the equipment oven for 1 minute. 2µL of a capture antibody solution (360µg/mL anti-human CRP capture antibody, 1X PBS, 1% w/v BSA) was dotted onto each test zone of the NC membrane and was dried at 37°C for 30 minutes. The NC membrane was washed three times in sterile petri dishes using the dilute washing buffer (1X PBS with 0.05% Tween 20) to remove excess antibodies. To fit the membrane into petri dishes, the membrane was carefully cut with scissors at the cutouts. The membranes were placed in a new sterile petri dish filled with 3% w/v BSA in PBS and incubated on an orbital shaker for one hour (70 rpm, 23°C, 1 hr). The membranes were washed once with 1X PBS buffer and twice with DI water to remove excess reagents. The membranes were dried a second time at 37°C for 30 minutes. Each test immunodot was carefully cut using scissors and carefully transferred to the extra thick blotting paper using high precision tweezers.

Immunodot assay:

5µL of a solution containing CRP standard was dotted onto the test zone and allowed to dry for 30 minutes. The CRP standards (2.0µg/mL, 1.6µg/mL, 1.2µg/mL, 0.8µg/mL, 0.4µg/mL, 0.2µg/mL, 0.1µg/mL, 0.05µg/mL, and 0.02µg/mL) were dissolved in 1X PBS with 1% BSA w/v. The CRP control was a 5µL dot of 1X PBS with 1% BSA w/v. Each test zone was then washed with 10 µL concentrated washing buffer (10X PBS 0.25% Tween 20) followed by 400 µL of DI water. The test zones were dried for 30 minutes. 5µL of the stock CRP detection antibody was dotted onto the test zone and

allowed to dry for 10 minutes. The stock CRP detection antibody was made 20 minutes prior to be used and was made by mixing 1.0 µL of 2mg/mL ALP-Streptavidin, 99 µL of 1X PBS in 1% BSA w/v, and 100 µL of 16.2 µg/mL biotinylated anti-human CRP antibody dissolved in 1X PBS in 1% BSA w/v. Each test zone was washed with 10 µL concentrated washing buffer, again, followed by 400 µL of DI water. The test zones were dried for 30 minutes. One BCIP/NBT tablet was dissolved in 10 mL to create the working substrate solution. 10 µL of the working substrate solution was dotted onto the test zones after the second washing step. Each test zone was allowed to sit on the blotting paper for 30 minutes to allow the ALP enzymatic reaction to finish. After 30 minutes, a smartphone picture was captured and uploaded to ImageJ software (US National Institutes of Health). Each picture was meticulously taken to avoid casting a shadow over the test zones, thereby impacting the detected colorimetric output.

2.5 Image Processing

Test zone analysis using ImageJ was identical to the procedure written by Verma, et. al.[27] Pictures of the test zones were first inverted to their negative using Adobe Photoshop before being uploaded to ImageJ. The RGB color values of a circle with a diameter of 25 pixels in the center of the test zone in the sensing area was measured. The color intensity from each of the R, G, and B channels was averaged to obtain the average intensity. This value was reported as the "RGB mean intensity" or the "colorimetric output".

3. RESULTS

3.1 RGB Mean Intensities

The red-green-blue (RGB) mean intensity output of the CRP control was compared to every reference standard using z-score evaluation to generate p-values for the CRP ELISA Immunodot procedure (Figure 3). Each CRP standard generated a statistically greater RGB colorimetric output than the control (Figure 3.1A). Representative qualitative illustrations (Figure 3.1B and 3.1C) highlight this principle. This is a very important analytic technique for an ELISA immunodot assay because many tests require qualitative user judgement. While the control depicts a few clear false positive dots, the vast majority of control strips had very minimal purple color formation.
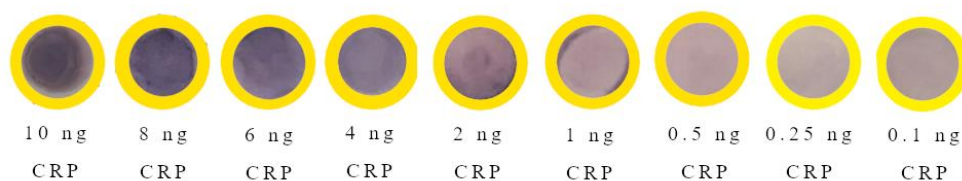
A.
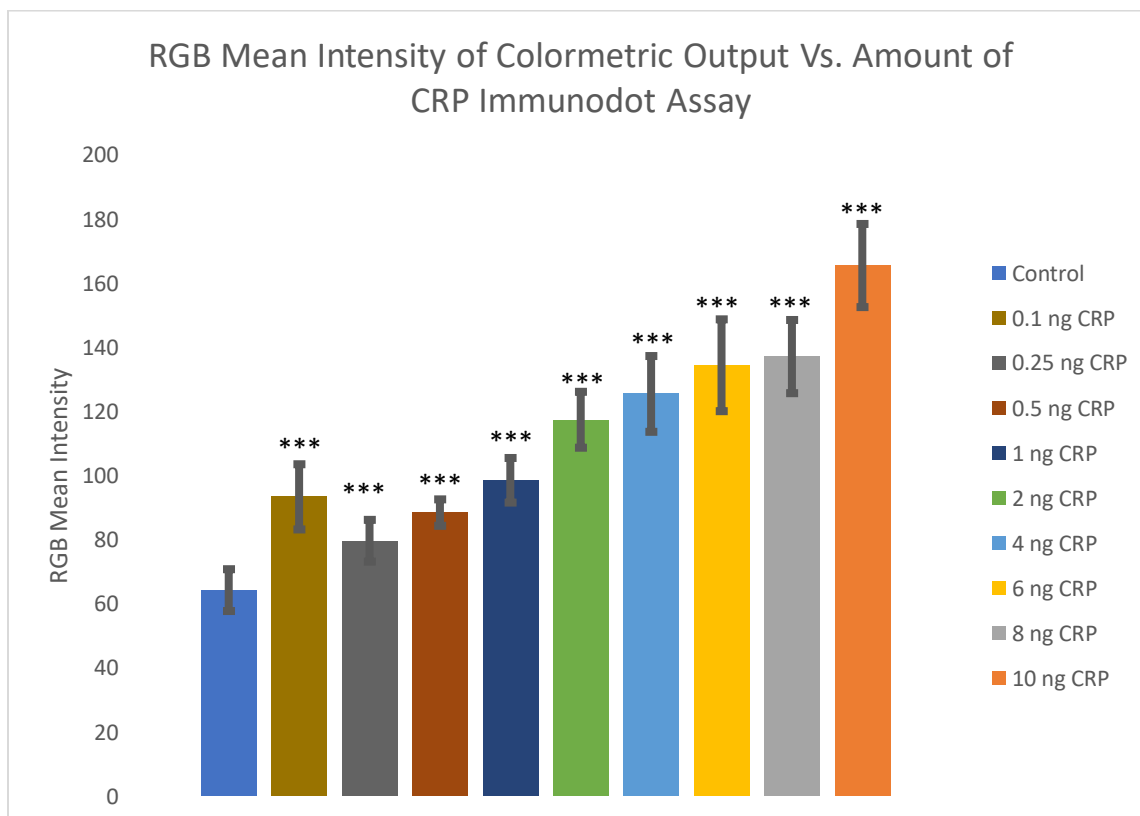
B.

C.

Figure 3.1 RGB Mean Intensities and representative examples A.) The colorimetric output of CRP standards (10 ng, 8 ng, 6 ng, 4 ng, 2 ng, 1 ng, 0.5 ng, 0.25 ng, and 0.1 ng) are compared to the control (0 ng CRP). Error bars indicate 95% confidence intervals. Eight measurements were taken at each CRP standard, except the 10 ng sample that had nine measurements. The control bar is the weighted average of the 86 samples. *** Indicates p<0.001. B.) Representative images for each standard CRP concentration. The image selected for this figure had the RGB intensity closest to the mean of the group colorimetric output. C.) Image of all 86 controls run in the experiment on a sheet of blotting paper.

All protein standards were quantified as a mass rather than a concentration. This was purposeful since the Discussion reframes this CRP ELISA immunodot for theoretical use at different blood dilutions as a screening tool for cardiac risk stratification (lower CRP levels) and acute inflammation (higher CRP levels).

3.2 Receiver Operator Characteristic (ROC) Curves

To determine the colorimetric output cutoff for FP/FN and to determine the quality of the plot versus the control (specifically if a certain CRP standard should be used in the calibration curve), a receiver operator characteristic (ROC) curve was generated to detect the diagnostic ability of the ELISA immunodot in response to a changing discrimination threshold. Performance was measured using the area under the curve (AUC) with 1 representing a perfect test and 0.5 (the diagonal line) representing classifiers without predictive values. Importantly, the colorimetric cutoff was selected as the apex of the ROC plot with the lowest AUC.

The ROC curve derived from combining all CRP standards had an AUC = 0.88 (Figure 3.2).
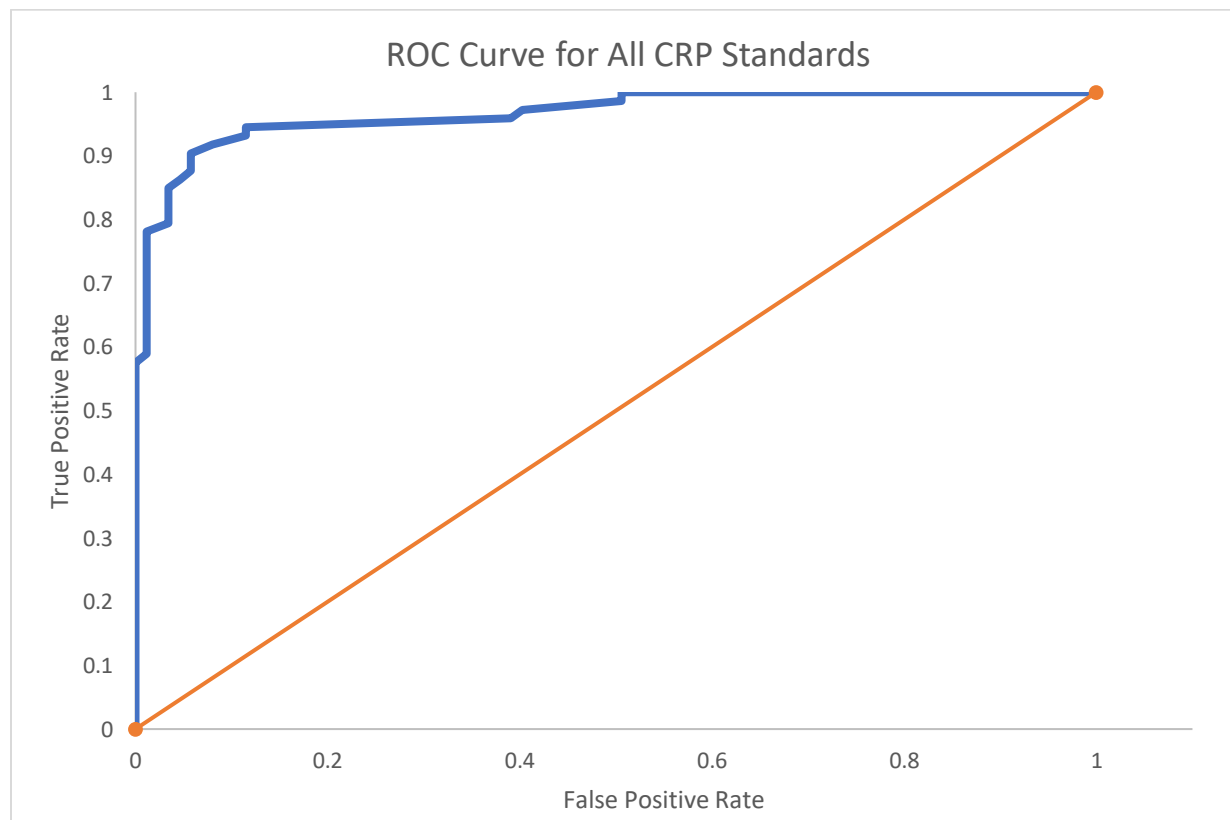
Figure 3.2 – ROC curve for all CRP standards (blue line). The AUC of 0.88 was estimated using a best fit of sixth degree polynomial and Simpson's rule. The orange diagonal line represents the classifier without predictive value line.

The curve was generated by picking critical RGB mean intensity outputs and counting the number of true positives from the CRP standards and counting the number of false positives from the CRP control at each critical colorimetric output. The X-Y scatter plot was connected.

While it combines all CRP standards, the ROC curve in Figure 3.2 indicates a borderline outstanding diagnostic test. The AUC was measured using Simpson's rule. Simpson's rule uses a best fit quadratic polynomial and approximates the AUC by integration:

$$\int_{x(i)}^{x(f)} f(x)\, dx = AUC$$

Equation 3.1 – Simpson's Rule. *f(x)* is the best fit quadratic polynomial, in this case, the ROC plot. Since the false positive rate for any discrimination threshold must be in the range 0-1, *x(f)* = 1 and *x(i)* = 0. All best fit polynomials for ROC curves in this thesis are degree 6 and were measured in Microsoft Excel.

While this curve demonstrates that the combined data can generate a high AUC, it provides little commentary on whether or not all CRP standards should be included in the calibration curve. Thus, the next step it to generate and evaluate a ROC curve for each CRP standard and quantify individual AUCs to determine if each CRP standard can be accurately separated from the CRP control.
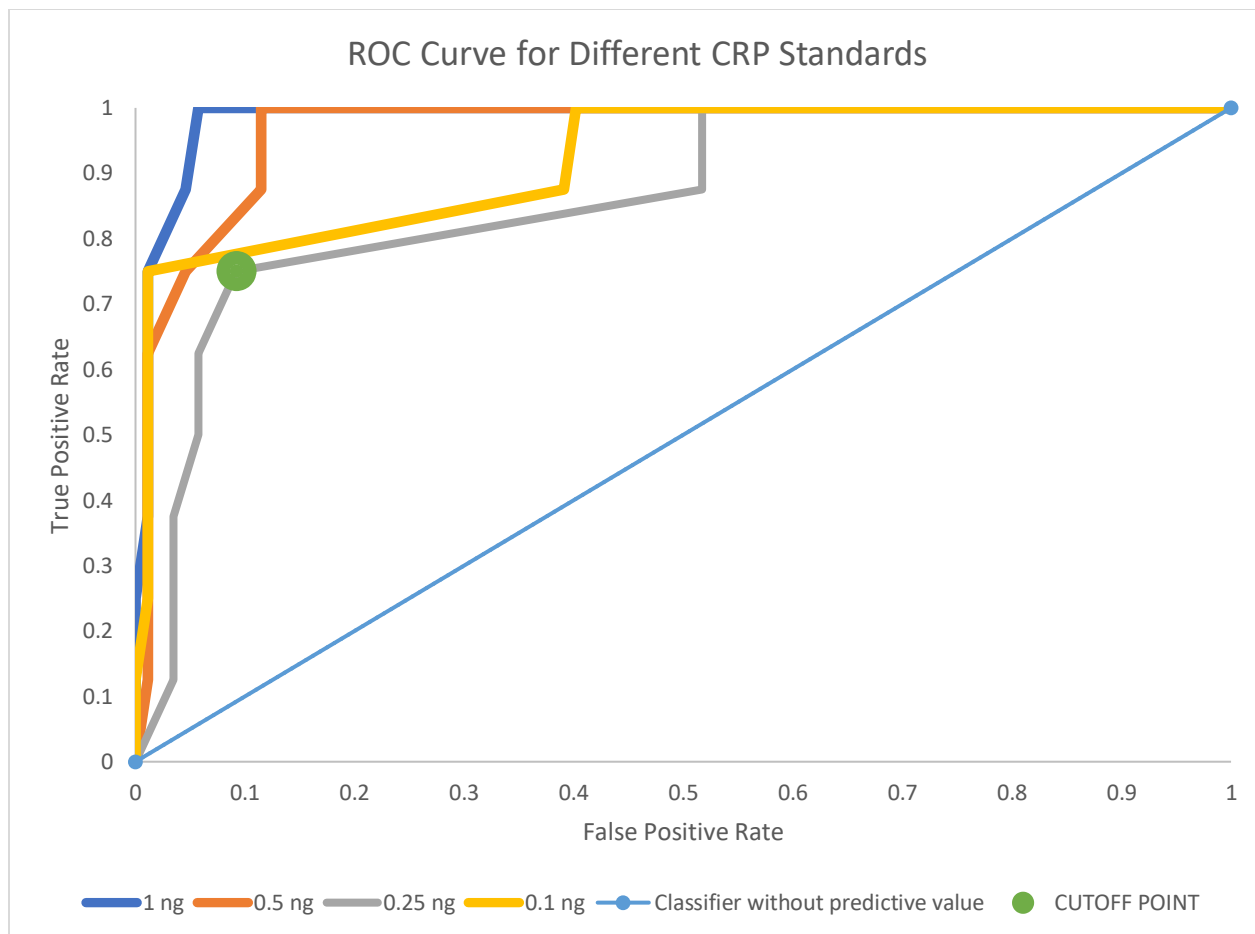
Figure 3.3 – ROC plot for the CRP standards 1 ng, 0.5 ng, 0.25 ng, and 0.1 ng Each of the standards from 10 ng through 2ng all had perfect ROC plots and were therefore not drawn. The curves were generated in an identical fashion to the one described in Figure 3.2. The AUC for each best-fit 6th degree polynomial is 0.97, 0.96, 0.96, and 0.96 for the 1 ng, 0.5 ng, 0.25 ng, and 0.1 ng standards, respectively.

Since all ROC plots generated outstanding AUCs, every CRP calibration point should be included in the calibration curve. Even though the 6-degree polynomial generated identical AUCs for the 0.5 ng, 0.25 ng, and the 0.1 ng sample, the grey line (0.25 ng CRP) was clearly identified visually as the one with the lowest AUC. Simpson's rule can have a considerable amount of error because the eight CRP standards only allow eight unique data points before the true positive rate reaches 100%. Since the

0.25 ng standard has the smallest AUC, it was used to determine the discrimination threshold as a conservative approach. If the discrimination threshold were picked from a higher CRP colorimetric output (e.g. any concentration greater than 0.25 ng CRP, including 0.1 ng CRP because it measured greater colorimetric output than 0.25 ng CRP), the data from all lower colorimetric outputs would be flawed. The proper discrimination threshold is the RGB value that maximizes the sensitivity and minimizes the false positive rate for all colorimetric outputs. Therefore, since the mean RGB output of the 0.25 ng CRP sample is closest to the control, the total number of false positives and false negatives across all standards/controls were minimized.

The threshold represented by the green dot (Figure 3.3) had a RGB colorimetric output of 81.427. However, since the 81.427 RGB output for the 0.25 ng CRP sample is just slightly below the apex of the ROC apex (a visual approximation), this value was considered a true positive for sensitivity and specificity calculations.

3.3 Sensitivity/Specificity Calculations

Following the methodology described above, of the 73 reference standard CRP positives, 67/73 were true positives (sensitivity 91.8%: 9/9 sensitivity at 10 ng CRP, 8/8 sensitivity at 8 ng CRP, 8/8 sensitivity at 6 ng CRP, 8/8 sensitivity at 4 ng CRP, 8/8 sensitivity at 2 ng CRP, 8/8 sensitivity at 1 ng CRP, 6/8 sensitivity at 0.5 ng CRP, 6/8 sensitivity at 0.25 ng CRP, and 6/8 sensitivity at 0.1 ng CRP) and 6/73 were false negatives (8.2% false negative rate). Of the 86 CRP controls, 83/86 were true negatives (specificity 96.5%) and 3/86 were false positives (3.5%). These results indicate the

immunodot assay has the potential to be a clinically meaningful tool in screening for CRP+ and CRP- patients.

As described in more detail in the Discussion, CRP is a regulatory blood serum protein that normally exists at 0.8 mg / L[6]. Therefore, no patient will truly be "CRP-". This heavily skews the data at any human sample dilution. However, the high sensitivity and specificity of this ELISA immunodot procedure are very promising as a proof-of-concept. What would likely occur if this immunodot was applied to a physiological blood sample is that the threshold of CRP standard would have to increase and consequently, the range of the calibration curve might be slightly reduced.

3.4 Calibration Curve

While this proof-of-concept check illustrates a well-conducted immunodot procedure, the notion "CRP+" and "CRP-" has limited clinical applications. Many rapid tests only require the granularity of "positive" or "negative" result, such as the BinaxNOW RAD COVID test that allows infected patients to isolate, thereby minimizing the spread of the virus. For CRP, it is much more important to know quantitative or semi-quantitative CRP blood concentrations. This could allow health care professionals to properly categorize each patient into the proper cardiac risk stratification group or into the appropriate degree of acute inflammation subset. This can be attempted using a calibration curve. It is worth noting that any immunodot calibration curve is likely going to be predisposed to a great deal of error because the assay itself is better suited for simply "positive" or "negative" results.

Figure 3.4 is a calibration curve generated by relating the mean colorimetric output for each CRP standard to the mass of CRP added to each immunodot.
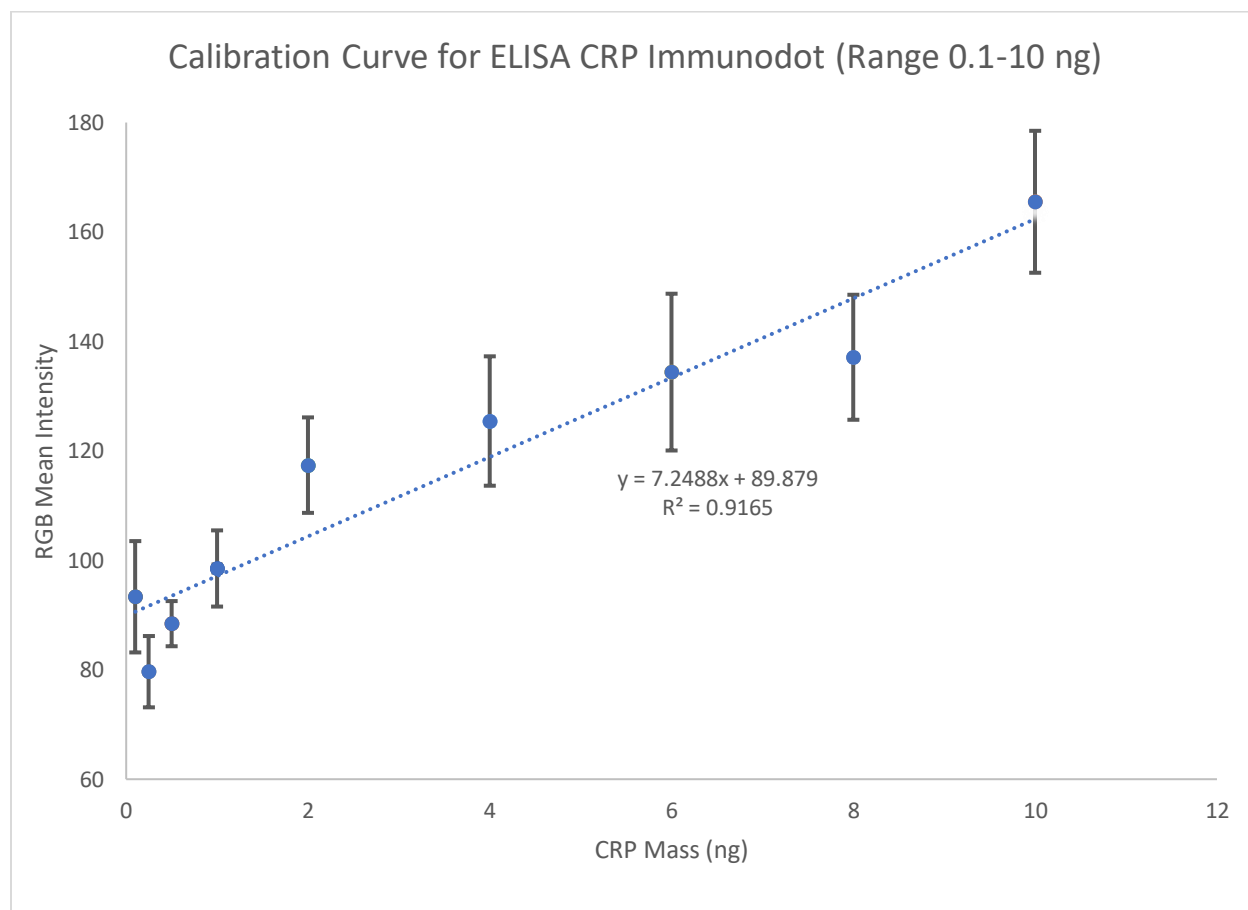
Figure 3.4 – The scatter plot of the mean RGB mean intensity, shown with 95% confidence intervals versus the mass of CRP standard added to each immunodot.

The slope of the calibration curve was 7.2±0.8 and the intercept was 90±4 with an R^2 of 0.92. The results indicate a fair agreement between RGB colorimetric intensity. However, it is somewhat disconcerting that the error bars from the 2 ng sample, the 0.5 ng sample, and the 0.25 ng sample are not within the best fit slope. The calibration curve has a considerable amount of room for improvement, but this was expected

because the immunodot assay was run in the solid phase rather than in aqueous

solution.

4. DISCUSSION

4.1. PoC Testing/Cost Analysis

Most US Healthcare facilities likely incorporate some form of PoC testing, depending on their clinical needs. A 2014 review article[41] postulated that countries would face pecuniary pressures to reduce healthcare spending by condensing expensive care into larger hospitals. PoC testing greatly alleviates the massive financial burden of some of the more expensive lab-based experiments.

There are two general PoC strategies. The first category is "scaled down" lab instruments. The Roche Diagnostics cobas® c111 mentioned in the Introduction can technically be used on a desktop. It runs many of tests that can be obtained by the larger, comprehensive cobas® 8100 series machine that requires a dedicated room and waste system, as well as specialized healthcare providers and staff[42] Miniaturized bioreactors like the c111 test sample volumes that are less than 100 milliliters. Depending on the model and manufacturer, there are both stirred tank reactors and shaken systems, for example, shaken flasks and microtiter plates[43].

This project focused not on scaled down instruments, but the second category – those that are smaller and potentially handheld. These smaller devices provide qualitative measures (positive or negative determination) and/or quantitative measures. Handheld devices allow patients and minimally trained personnel the ability to obtain consistent, reliable, and rapid results. Integrated microfluidic biosensors are promising to fill this role[44]. These devices can use very small sample sizes (as low as one

nanoliter) and there can be mass production, low reagent consumption, and few or no hazardous materials. One drawback to microfluidics, as described in the Introduction is that device fabrication can be expensive for many solid phases because the fabrication of high-resolution channels in solid supports often require advanced machinery and a lab based setting. Accordingly, paper-based microfluidics have gained a great deal of attention throughout the scientific community.

The World Health Organization (WHO) has designated µPADs as a key components of ASSURED (affordable, sensitive, specific, user-friendly, rapid and robust, equipment-free, and deliverrable) protocol[25]. This form of testing remains among the most promising applications of paper microfluidics. With micro- and nano-structures inside, sophisticated paper constructs can serve as a scaffold for cellular microenvironments. Paper can be used for cell-related biochemical analysis, such as the detection of small molecules like CRP, as well as DNA/ RNA complexes[25]. µPADS tend to be lightweight, easily disposed, and the can be designed to conduct tests using no external power source. Most importantly, these devices are very inexpensive.

Even though the CRP ELISA immunodot experiment in this thesis was neither microfluidic nor PoC, it was entirely paper-based and therefore very inexpensive. In fact, the approximate price per test zone (not including the CRP Standard) was $1.73. This is an affordable assay and CRP ELISA immundots/microfluidic platforms, such as the one conducted in this thesis, may have future clinical relevance in a finance-limited setting.

Table 4.1- Cost analysis for all materials used to determine the price per unit of each ELISA Immunodot.

Kit/Reagent	Cost ($)	Technique	Number of Tests per Kit/Reagent	Price Per Test
Speedball Advanced All in One Screen Printing Kit (Amazon)	$99.99	The photolithographic plate is generated onto a mesh substrate and ink can be pushed through. Approximately 100 prints can be conducted on the mesh*	19200	$0.0052
Rapid Cure Plastisol Ink Black (8 oz)	$10.99	Each container of ink mixed with reducer generates approximately 20 prints.	3840	$0.0029
Victory Screen Printing Plastisol Ink Reducer/Detackifer (quart)	$13.99	The reducer was approximately mixed in a 65:35 ratio with plastisol ink[26]. Thus, roughly 15 oz of plastisol ink were used per container of plastisol ink.	8270	$0.0017
Nitrocellulose Membrane, Precut, 0.45µm, 20x20 cm (BioRad)	$141.00	Package of 5 NC membranes. Each membrane produces 192 test zones	960	$0.1469
BSA Product A7030, 50 grams	$371.00	BSA is needed in the device (2 mg per capture antibody dot, 5 mg per recombinant CRP dot, 2.48 mg per detection antibody dot) and in the washing buffer (each membrane requires approximately 75 mL of 3% BSA). Thus, each individual test requires a total of 20.95 mg BSA.	2386.6	$0.1554
OmniPur 10X PBS Liquid Concentrate, 4L (Sigma Aldrich 6505-OP), 4L	$167.00	Approximately 81 mL of PBS 0.05% Tween is needed to wash excess capture antibodies after the first drying step. Approximately 27 mL of PBS is needed to wash the capture antibodies after the orbital shaking step. Each individual test uses 20 µL 10X PBS 0.25% Tween. Thus, approximately 583 µL 10X PBS is needed per test.	6861.1	$0.0243
Tween® 20 (Sigma Aldrich P1379-25mL)	$14.10	Approximately 81 mL of PBS 0.05% Tween is needed to wash excess capture antibodies after the first drying step. Each individual test uses 0.26µL Tween 20.	119047.6	$0.0001
R&D CRP ELISA Kit (DY 1707)	$679.00	45 µg of detection antibody and 360 µg of capture antibody were shipped in the kit. 720 ng of capture antibody were loaded onto each NC test zone and the detection antibody dot contained 40.5 ng of detection antibody. The capture antibody reserve can dot 500 NC test zones and the detection antibody stock has enough detection antibody for 1,111 test trials. Thus, the kit itself can be used 500 times.	500	$1.3580
Streptavadin-labeled ALP (Thermofisher S921)	$368.00	The Streptavidin-ALP comes in a 2 mL stock solution at 0.5mg/mL. The streptavidin ALP stock is added to the capture antibody in a 1:200 dilution. Thus, 5µL of detection antibody solution contains 50 ng of Streptavidin-ALP.	20000	$0.0184
BCIP/NBT Tablets (Sigma Aldrich), 20 tablets	$123.00	BCIP/NBT tablets were dissolved in 10 mL of DI water. 10 µL of BCIP/NBT solution was used for the readout. Thus, each tablet can be used for 1,000 runs.	20000	$0.0062
BioRad Blotting paper Catalog no. 1703969, Pack of 30	$70.00	Each sheet of blotting paper could accommodate 1 NC Test sheet	5760	$0.0122

4.2 Limitations

The original methods for this project were based on a successfully published sliding strip µPAD[27]. The device from the index paper[27] relied on capillary action both horizontally (inside the hydrophilic layer) and vertically (connecting hydrophilic sections allowed the passage of fluid). To control both horizontal and vertical capillary action, hydrophobic barriers must be printed *into* the paper substrate. This means that water cannot escape the fabricated channel at any height within the paper substrate (Figure 4.1)
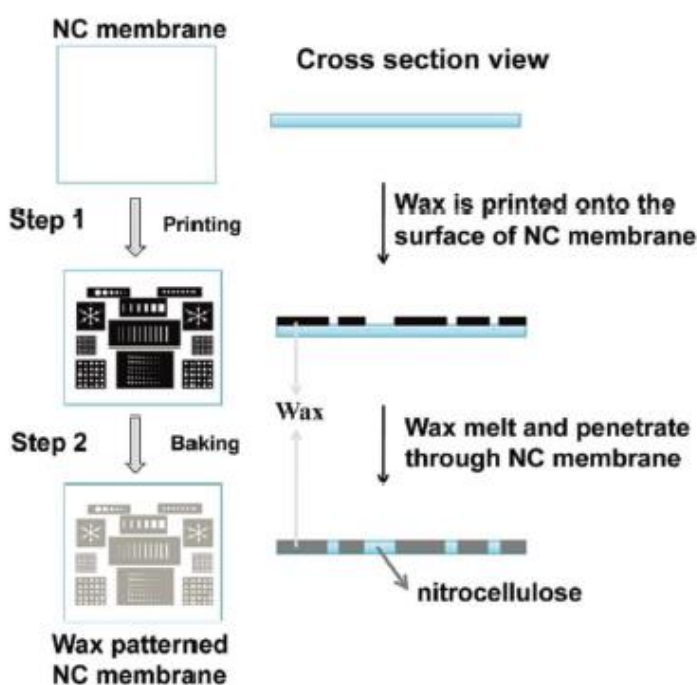

Figure 4.1 – Schematic for baking wax/ink into paper layers[25].

In Figure 4.1, the wax completely penetrates the nitrocellulose membrane. This is the typical procedure to fabricate hydrophobic channels in a paper substrate using a wax printer. The Whitesides Lab used this methodology for their µPAD fabrication[27].

However, as mentioned above, Bard College does not have access to a wax printer. To bypass this issue, I attempted to melt plastisol PVC ink into the paper substrate (using a heat gun), suggested by Sitanurak, et. al.[26]. The authors reported that "for PP and PVC inks the pigments can be transported with the organic solvent [through the paper] better than all 'water-based inks' as observed for Whatman No. 1" [26] and "the PVC ink completely prohibited leakage of the aqueous dye indicating good hydrophobicity" [26]. Additionally, a qualitative figure was provided to demonstrate the high penetration efficiency of the PVC ink[26].
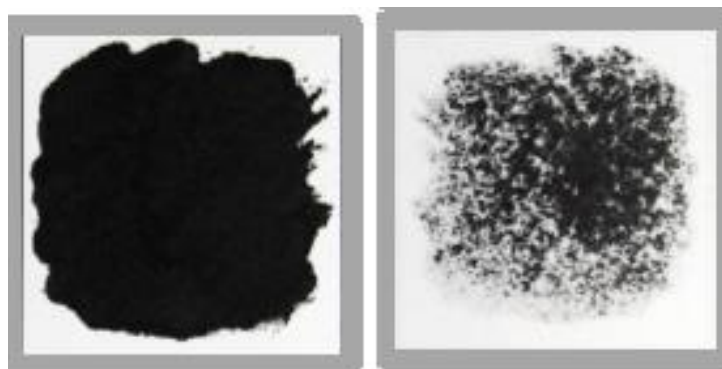

Figure 4.2 – PVC penetration efficiency, as reported by Sitanurak, et. al.[26] The left figure is the front of the paper (where screen printing occurred) and the back is the underside of the Whatman No. 1 paper melting the ink into the paper.

These results could not be reproduced. Specifically, the solvent-based inks could not be transported at all through either paper substrate (Whatman No. 1 chromatography paper nor nitrocellulose). In fact, the water-based inks tended to penetrate the chromatography with slightly better efficiency than the solvent-based inks. However, both inks were very far from being usable in μPAD. Results of the "water test" (100μL of red food coloring was spotted onto inlet zone one, where the blood sample is supposed to be added) can be seen below (Figure 4.3):

Figure 4.3- This image shows the backside of the splitting layer after dissection of the failed µPAD during the "water test". This µPAD used PVC-based plastisol ink.

The food coloring provides a nice visualization of what happens to the moving solution and why the device fails; the solution rapidly spreads on the backside of splitting layer because no hydrophobic channels penetrate the paper, thereby allowing for random diffusion. Consequently, the food coloring did not elute down onto the test strip and no food coloring was able to pass the splitting layer. Moreover, Figure 4.3 demonstrates the nonexistent PVC ink penetration of the paper layer.

The most likely reason the screen-printing experiment failed is a result of the chemical makeup of the screen-printing ink. Plastisol ink is a suspension of PVC resins among other organic molecules that cross link at thermosensitive temperatures (typically 149°C-166°C)[32]. There is no set formula to make plastisol ink, the only requirements are that the ink must have PVC resins and molecules that will plasticize. Therefore, companies tend to sell their own plastisol ink formulas, which is not typically released to the public. Additionally, the plastisol reducer is any solvent that decreases the viscosity of the ink to increase ink-mesh permeability. Accordingly, different plastisol ink-reducer combinations may have different chemical properties. When printing with on a T-shirt the chemical properties of the ink are of little concern as long as the dye can

be seen on the shirt. However, when fabricating a µPAD, the chemical makeup of the ink is paramount because the ink must successfully penetrate the paper.

Additionally, detailed methodology/data describing the capillary action of the devices fabricated by Verma, et. al.[27] and Sitanurak, et. al.[26] was not provided for either paper. It may have been that very controlled paper flow was available in the Whitesides Lab, but the details of how flow was regulated were otherwise not included in the written methods. In retrospect, it was perhaps naïve to believe that capillary action alone would follow the intended vertical flow patterns among successive layers to yield reliable results in the initial phases of these experiments, especially considering that a completely different mechanism was used to fabricate hydrophobic barriers. Many successful paper-only devices used patented products (such as the home pregnancy test). The details of the exact paper combinations are often restricted to the manufacturer. That being said, the Whitesides lab is recognized for integrity and forthrightness, and to be optimistic, I believe that if equipped with a wax printer, I would have been able to successfully fabricate the µPAD.

Accordingly, the main limitation of this project was that the experiments were simplified to an ELISA immunodot on a single nitrocellulose layer. Unfortunately, not only does this experiment fail to fabricate a µPAD, but also no longer deals with paper microfluidics nor PoC analysis (the immunodot requires lab-based reagents stored in an industrial -80°C freezer, thereby making this test inaccessible outside of the lab-based setting). However, this strategy was both pragmatic and successful in obtaining CRP+ and CRP- samples and in generating a calibration curve that related the mass of CRP dotted onto the immunodot to the RGB colorimetric output.

The next four limitations focus on the experiment as performed and its applicability. First, the data set does not include broad ranges of measurable CRP blood concentrations, rather the results simply relate colorimetric intensity to the mass of CRP added to the sample. To take on this limitation, the next section of the Discussion assumes that a dilution method can be performed; it suggests how CRP testing could span boarder clinical ranges of an inflammatory response by strategically diluting different blood concentrations. Admittedly, only the singular set of data is used, but this additional works shows how the project can be imagined for further applicability.

However, the impact of blood serum is not accounted for; all samples were made without the preparation of sheep's blood (as the Whitesides research group does[27]). Therefore, the dilution method could be seriously flawed if some off-target sticking occurs between the blood serum and the capture antibody/detection antibody. Second, the actual experiments took on the order of hours to complete; if presented with a clinical case the determination of CRP would have been easier and quicker by using a commercial system. Third, it would have been interesting to run the samples on a clinical "desktop" device such as the Roach cobas® c111 as a comparator as a reference standard. Forth, varying degrees of ambient light can influence the RBG colorimetric output. No standard methodology was reported in this thesis to normalize the ambient light in different trials.

Despite the limitations, the CRP ELISA immunodot provides one advantage relative to the index paper used as a reference. This advantage is that the Whitesides Lab used a blank section of NC test zone as the control. The control for this immunodot

assay adds a sample without CRP to a NC test zone coated in capture antibody. Thus, the RGB colorimetric output of the control accounts for random off-target sticking.

4.3. Data Extrapolation to Clinically Relevant CRP Values

As mentioned above, the failure to fabricate a usable µPAD changed the detection platform from a paper-based microfluidic device to an ELISA immunodot assay. Colorimetric ELISA immunodots, such as ABO blood typing, are clinically used for qualitative analysis only. For example, in ABO blood typing, if a patient is blood type A, the anti-A mAbs adhered to the solid phase in well A will bind to antigen A on his or her RBCs (ultimately leading to a positive ELISA test), but the anti-B mAbs adhered to the solid phase in well B will not be able to form the antibody-antigen-antibody sandwich with the patients RBCs (ultimately leading to a negative ELISA test). The positive/negative color change is visualized directly and reported by the test administrator.

Thus, as a proof-of-concept immunodot assay, the most important aspect of this experiment is to determine the sensitivity and the specificity of the assay. In other words, can this CRP ELISA immunodot assay reliably detect CRP+ and CRP- samples? A secondary goal is to determine if an unknown colorimetric output can effectively predict unknown CRP blood concentrations using a calibration curve.

The data acquired over the RGB mean intensities showed that CRP can be reliable measured as a PoC "CRP+ versus CRP-" device. However, as mentioned earlier grouping patients in terms Cardiac Risk/ Inflammatory Events based on their measured CRP blood concentration is much more clinically relevant. The calibration curve (y= (7.2

± 0.8) x + (90 ± 4)) relates the RGB colorimetric output (y) to the mass of CRP in nanograms (x). Thus, it is reasonable to expect that when the sample containing CRP is strategically diluted, the colorimetric output of the test may be able to predict low, medium, and high-risk cardiovascular groups and normal, mild, moderate, and severe acute inflammation groups using clinically relevant cutoffs.

Since the immunodot calibration curve had a fair degree of error, an indeterminate region is located between each cardiac risk cutoff and each inflammatory event cutoff. This indeterminate region is calculated using the error on the calibration curve. For example, in the low-medium indeterminate region for hypothetical cardiac risk stratification table, the lower bound calibration curve is used to attain the lower bound colorimetric output (92.2 = 6.4*1 + 86) and the upper bound colorimetric curve is used to attain the upper bound colorimetric output (102.1 = 8.0*1 + 94). Note, in the calculations above, more significant figures are used in the actual calculations, thereby generating answers that might otherwise appear slightly incorrect.

Table 4.2 - Hypothetical Cardiac Risk Stratification Sample Preparation Strategy. All sample dilutions are identical.

Relative Risk Level	CRP concentrations (mg L^{-1})	Sample Preparation	Volume of sample added to test zone (μL)	Mass of CRP Added to Immunodot (ng)	Colorimetric output Range (RGB mean intensity)

Low	Less than 1	1 Parts Blood Plasma dissolved in 4 parts PBS 1% w/v BSA	5	Less than 1	0-92.2
Low-Medium Indeterminant	Could be Less than 1 or 1-3	1 Parts Blood Plasma dissolved in 4 parts PBS 1% w/v BSA	5	Could be Less than 1 or 1-3	92.2-102.1
Medium	1-3	1 Parts Blood Plasma dissolved in 4 parts PBS 1% w/v BSA	5	1-3	102.1-105.0
Medium-High Indeterminant	Could be 1-3 or 3+	1 Parts Blood Plasma dissolved in 4 parts PBS 1% w/v BSA	5	Could be 1-3 or 3+	105.0-118.2
High	3+	1 Parts Blood Plasma dissolved in 4 parts PBS 1% w/v BSA	5	3+	118.2+

This suggests a potentially promising application of the ELISA immunodot assay in this thesis for cardiac risk stratification. Low, medium, and high-risk groups all have corresponding colorimetric outputs. The drawback is that the range of the indeterminate groups are much larger than the range of the medium group (the only risk group with upper and lower boundaries). Before such a device could be used in the clinical setting, the range of the indeterminate regions would need to significantly decrease and the range of the medium risk would have to significantly increase.

It is also important to note that while CRP is an established, proven biomarker for inflammation, its use a screening tool for cardiovascular risk remains controversial. While there is a large literature to support its use[2], the support is not universal.

The United States Preventive Services Task Force (USPSTF) serves Americans by creating guidelines for disease prevention. USPSTF members are volunteers who are experts in public health and those medical specialties for which they contribute to the recommendations. Since 1998, the USPSTF has been supported by the US Agency

for Healthcare Research and Quality, a federally funded organization with

Congressional oversight[45].

In 2018, the Task Force considered three tests that are commonly used for

cardiac assessment: CRP, coronary calcium scoring (determined by a computed

tomography scan of the heart), and ankle-brachial index (determined by serial blood

pressure measurements with inflation cuffs used to screen for disease of the arteries in

the legs)[45]. That USPSTF grouped these three tests as cardiac "nontraditional risk

assessments" and then published the following, "the current evidence is insufficient to

assess the balance of benefits and harms of adding" these three test for all

Americans[45]. The recommendation to test large groups of Americans – or any

population, has widespread consequences since the cost of the test and the ability for

wide distribution must be considered. Despite these formal recommendations, all three

of these tests are ordered quite frequently. It is difficult to quantify how many times CRP

is used for cardiac risk scoring, since its overall use in medicine is so ubiquitous.

Categorizing acute inflammation groups is more challenging because CRP blood

concentrations can rapidly increase 1000-fold[2, 6, 27] and the calibration curve of this

thesis has a range of 100X (0.1 ng CRP – 10 ng CRP). However, a mild inflammatory

response is considered to correspond with CRP concentrations above 10 mg / mL and

any severe inflammatory event to correspond to a CRP concentration greater than 200

mg/mL[2]. Thus, even though the physiological response can be 1000X, only a 20X snip-

it of that response is needed for PoC clinical groupings. Accordingly, the upper limit

severe infections will fall into the nonlinear region of the calibration curve due to the

hook effect. For these hypothetical patients, CRP cannot be accurately quantified, other than being designated as "severe".

Table 4.3 - Hypothetical Inflammatory Response Groupings. All sample dilutions are identical.

Intensity of Inflammatory response	CRP concentrations (mg L^{-1})	Sample Preparation	Volume of sample added to test zone (µL)	Mass of CRP Added to Immunodot (ng)	Colorimetric output Range (RGB mean intensity)
Normal, no significant inflammatory event detected	Less than 10	1 Parts Blood Plasma dissolved in 110 parts PBS 1% w/v BSA	5	Less than 0.5	0-88.7
Normal-Mild Indeterminant	Could be Less than 10 or 10-40	1 Parts Blood Plasma dissolved in 110 parts PBS 1% w/v BSA	5	Could be Less than 0.5 or 0.5-1.8	88.7-97.6
Mild-Moderate Indeterminant***	Could be 10-40 or 40-200	1 Parts Blood Plasma dissolved in 110 parts PBS 1% w/v BSA	5	Could be 0.5-1.8 or 1.8-9.0	97.6-108.5
Moderate	40-200	1 Parts Blood Plasma dissolved in 110 parts PBS 1% w/v BSA	5	1.8-9.0	108.5-143.6
Moderate-Severe Indeterminant	Could 40-200 or 200+	1 Parts Blood Plasma dissolved in 110 parts PBS 1% w/v BSA	5	Could be 1.8-9.0 or 9.0+	143.6-166.7
Severe	200+	1 Parts Blood Plasma dissolved in 110 parts PBS 1% w/v BSA	5	9.0+	166.7+

*** The mild upper limit (93.3 = 6.4*1.8 + 86) was less than normal-mild indeterminant upper limit (97.6 = 8.0*0.45 + 94). Consequently, the mild lower limit was greater than the mild upper limit. Thus, there is too much error in the standard curve to accurately measure a mild inflammatory response. Consequently, this section has been excised from Table 4.3.

Similar commentary can be made for Table 4.3 as was said for Table 4.2; having the ability to group inflammatory response groups is exciting, but the range of the indeterminate is still far too large and the range of the risk groups with boundaries is far

too small (the mild group even had a negative range). Thus, further optimization would be needed before such a device could have any clinical significance.

Future research on such a topic would include the generation of ROC plots for each of the cardiac risk stratification groups and inflammatory response groups to obtain the sensitivity and specificity of this experiment. Assuming proper fabrication of the sliding strip μPAD, these sensitivities and specificities could have clinical relevance and could be used to determine whether or not a CRP immunodot assay described in this paper could help health care workers properly categorize CRP levels.

4.4. Future Directions in Cardiac Risk Assessment

Among these three tests defined by the USPSTF as "nontraditional" for cardiovascular risk, CRP is very different from the other two. Coronary calcium scoring and ABI measurements can only done by very highly trained medical professionals. Calcium scoring requires a CT scan and expensive professional interpretation fees[46], and ABI measurements are labor intensive and have high professional costs as well[47]. CRP is different, less expensive, and the opportunity for PoC testing is intriguing.

The results of this project support the hypothesis that - with further research and more sophisticated microfluidics paper, CRP testing could be further miniaturized. It is also reasonable to at least speculate that the readout is possible part of future mobile phone technology[48] that will use RBG input and output for a larger array of digital data transfer. One other piece of this puzzle is healthcare "empowerment apps" where patients can input and evaluate their own medical data. One example of this is a cell

phone app that not only provides data from the medical center to the patient, but also enables patients to engage in their own care by providing input themselves[49].

The assumption that a PoC device can provide accurate CRP readouts via a mobile phone and uploaded into a healthcare app like Opal is not far-fetched, although a standard photography technique would be needed to minimize the impact of different ambient lights that each patient would use for their image test. Perhaps more intriguing is that one could image a single larger lab on a chip for risk screening, where many different important biomarkers could be obtained by RBG intensity readouts. This data as well as other physiology parameters that obtained from wearable devices could be integrated in a format amendable for healthcare big data[50]. To date, there has been large volumes of physiology data available and propositions for artificial intelligence to capitalize on it[51] but converting this into meaning risk assessment is yet to be scientifically validated. Adding medical data such as CRP and other markers obtained from blood, urine and saliva may enable revolutionary healthcare products. The use of CRP in big-data applications would enable robust testing of the hypothesis that it provides useful risk stratification, and this would very likely move the needle among a group such as the USPSTF.

4.5. COVID-19: A Novel Device to Quantify Cytokine Storm

As noted in the Introduction, COVID-19 has catapulted PoC testing to become not only a matter of science, but also a matter of public health, economics, and even politics. The Abbott home COVID test discussed above is routinely used, including at Bard in the athletics department.

COVID-19 markers for disease severity and therapeutics have been clinically challenging because scientists do not fully understand the pathophysiology. While some patients have a more clinically benign respiratory viral syndrome, others become severely ill and die. It is not yet possible to *a priori* separate those groups, and thus public health officials have identified the elderly and those with pre-existing medical conditions as higher risk. However, younger patients die from COVID-19, and many elderly patients have proven remarkably resilient.

"Cytokine storm"[52] is now considered central to the COVID-19 morbidity and mortality. As of May 2, 2021, the US National Library of Medicine (NLM) (www.pubmed.gov) lists over 2,600 publications from the search string "Cytokine Storm COVID-19". The term "cytokine storm" is over a decade old. With respect to COVID-19 the phenomenon refers to the complex interaction of immune, inflammatory, and coagulation cascades after respiratory infection[53]. The clinical presentation includes hyperinflammation, hyperferritinemia, and end-organ failure resulting from overproduced cytokines in a positive feedback loop[54].

While the storm is well documented clinically, during a peak pandemic response, laboratory resources for any individual medical center are limited, and even basic testing can be difficult to perform, and at times, impossible. Three most commonly tested proteins during a serological "cytokine storm" are serum ferritin, CRP, and D-Dimer[53].

There is even growing evidence that CRP can also be a useful biomarker in COVID-19. A recent paper[55] shows that patients who need intubation and prolonged respiratory support first show a rapid rise in CRP. Patients with severe disease will have

CRP levels in > 200 mg / L, which represent the upper limit of the severe inflammatory response grouping. Ferritin is released at high rates by active macrophages and its production is increased by cytokines[56]. D-dimer is a degradation product of fibrin – it is detected after a clot has undergone fibrinolysis. Thus, D-dimer is a nonspecific marker of increased blood clotting. A large literature points to incremental increases for all three tests in proportion of COVID-19 disease severity[57-58]. While this screening panel (ferritin, CRP, and D-Dimer) is routinely obtained for COVID-19 in the US, where more resources are available, all three tests query downstream effects of the disease because they are highly sensitive.

The work in this senior project points to the feasibility of a PoC paper microfluidics test for this cytokine storm biomarker kit (CRP, ferritin, and D-Dimer) that can be done by patients in quarantine, in their own home immediately following diagnosis. Required reagents in addition to the kit outlined by the Whitesides research group would include recombinant heavy chain human ferritin (Cayman Chemical Item No. 32033), EPR3004Y recombinant anti-ferritin antibody (abcam Item No. 75973), ferritin antibody biotin conjugated (Rockland Antibodies & Assays Catalog No. 200-406-090-0100), recombinant human D-dimer (Sigma Aldrich Product No. D9321), 3B6 recombinant anti-D-Dimer antibody (abcam Item No. 273889), and DD2 D-Dimer antibody [Biotin] (Novus Biologicals and Biotech Catalog No. 8376B).

The blueprint for this theoretical device can be found in the Appendix (Appendices H-L). It has a very similar design to that of the Verma design[27]. The main difference is that each inlet zone is split into four distinct zones rather than two. The test zone, blown up in Figure 4.4 below, would have 4 immobilized dots.

Figure 4.4 – Test zone fabrication for hypothetical cytokine storm test panel. Note, these colors are not printed onto the paper, nor the colors of the enzymatic readout. Rather, the schematic is used to demonstrate where the capture antibodies can be added to the test strip.

If anti-CRP capture antibody is added to the yellow dot, anti-ferritin capture antibody is added to the red dot, anti-D-Dimer capture antibody is added to the blue dot (leaving the green as the control), chemical readouts at each dot will correspond to the presence (or lack thereof) of that particular antigen in the sample. Thus, when the sliding strip is in position 1 and the sample is wicked into zone 1 on the inlet layer, recombinant CRP, ferritin, and/or D-dimer will bind to its appropriate adsorbed capture antibody if it is present in the sample. Excess unbound proteins are washed by the washing buffer stored in the first inlet layer.

The detection antibody for each antigen (CRP, ferritin, and D-Dimer) would be prepared in the same fashion; Streptavidin labeled ALP would be added to the biotinylated anti-antigen antibodies in identical molar concentrations to create ALP labeled detection antibodies. ALP conjugated anti-CRP would be dried into the first hole in the storage layer, ALP conjugated anti-ferritin would be dried into the second hole in the storage layer, ALP conjugated anti-D-Dimer would be dried into the third hole in the storage layer, and all three detection antibodies would be dried into the final hole in the storage layer. Thus, when the patient pulls the sliding strip to position 2 and adds water

to the second inlet layer, detection antibody is eluted to the test zone. Excess unbound detection antibody is washed by the washing buffer in the second inlet layer.

Crushed BCIP/NBT would also be deposited in the splitting layer, identical to the Verma procedure[27]. When the patient pulls the sliding strip to position 3 and adds water to third inlet layer, the stored detection buffer is eluted and dissolved BCIP is delivered to the test zone. When the patient pulls the sliding strip out of the device, his or her blood CRP, ferritin, and D-dimer concentrations could be visualized to potentially determine the future clinical COVID-19 severity. Visualization techniques would be identical to those described by the immunodot assay that this thesis discusses.

The panel could be read out by a cell phone and uploaded to an app such as Opal. Such large data sets could provide breakthrough insights to COVID-19 care, or for a future pandemic. This readout would occur when clinical deterioration is unlikely and data is lacking.

It is important to note that device above quantifies three cytokine storm biomarkers, rather than the cytokines themselves. This assay is intended to closely monitor the inflammatory response. Better studies for the cause-and-effect of cytokine storm and COVID-19 mortality would directly test the cytokines themselves. Companies have embarked on selling such test kits, some with a "kitchen sink" approach for sandwich ELISA for those cytokines found at autopsy among COVID-19 patients, and some with a more selective approach. Many commercial products are currently marketed for COVID-19 research. One example is from Anogen "Multiplex Human Cytokine ELISA Kit (Inflammatory)". This kit ranges from $840 USD to $4,000 USD for simultaneous ELISA testing of Interleukin-1α, Interleukin-1β, Interleukin-6, Interleukin-8,

Interferon-γ, Granulocyte Macrophage Colony Stimulating Factor, Monocyte

Chemotactic and Activating Factor, and Tumor Necrosis Factor (TNF)-α.[59] Whether it is

the novel device proposed in this Senior Thesis or the Anogen product above, in order

for a product to be marketed and sold in the US on-label for COVID-19 intended use (in

this case testing and disease monitoring), it needs FDA clearance. This would typically

come as an Emergency Use Authorization (EUA) like the Abbott rapid test for COVID.

COVID-19 changes on a day-to-day basis, and at the time of writing this Senior Thesis,

it does not appear that the FDA has approved any cytokine-based test kits for clinical

monitoring during the pandemic. This is like why the Anogen product is marketed and

sold for biomedical research.

The lack of current EUA from the FDA does not and should not imply that there

are not many applications to the FDA. Cytokine research has intensified. While it is

important to cautiously avoid oversimplification and remain mindful of the complexity of

COVID-19 pathophysiology, at the same time clinical scientists must increase the flow

of data so that diagnoses and treatments can advance as rapidly and as safely are

reasonably achievable. PoC testing is an important method to increase that data flow.

4.6. Summary

ELISA-based CRP Immunodotting shows reliable human C-reactive protein

detection at concentrations important for human physiology and disease. With further

refinement (both in device fabrication when considering the failed μPAD and assay

development), there are implications for Point-of-Care testing for this biomarker, among

others. COVID-19 has spotlighted these rapid tests; they are now part of mainstream

culture internationally. With this attention, there is renewed, positive enthusiasm on developing and implementing inexpensive, convenient, and reliant medical devices for home use.

REFERENCES

1.   Tillett, W. S.; Francis, T., SEROLOGICAL REACTIONS IN PNEUMONIA WITH A NON-PROTEIN SOMATIC FRACTION OF PNEUMOCOCCUS. *J Exp Med* **1930,** *52* (4), 561-571.

2.   Ridker, P. M., C-reactive protein: eighty years from discovery to emergence as a major risk marker for cardiovascular disease. *Clin Chem* **2009,** *55* (2), 209-15.

3.   Mullenix, M. C.; Mortensen, R. F., Calcium ion binding regions in C-reactive protein: location and regulation of conformational changes. *Mol Immunol* **1994,** *31* (8), 615-22.

4.   Mortensen, R. F., C-reactive protein, inflammation, and innate immunity. *Immunol Res* **2001,** *24* (2), 163-76.

5.   Volanakis, J. E., Human C-reactive protein: expression, structure, and function. *Mol Immunol* **2001,** *38* (2-3), 189-97.

6.   Sproston, N. R.; Ashworth, J. J., Role of C-Reactive Protein at Sites of Inflammation and Infection. *Front Immunol* **2018,** *9*, 754-754.

7.   Ledue, T. B.; Rifai, N., Preanalytic and Analytic Sources of Variations in C-reactive Protein Measurement: Implications for Cardiovascular Disease Risk Assessment. *Clinical Chemistry* **2003,** *49* (8), 1258-1271.

8.   Roberts, W. L.; Moulton, L.; Law, T. C.; Farrow, G.; Cooper-Anderson, M.; Savory, J.; Rifai, N., Evaluation of nine automated high-sensitivity C-reactive protein methods: implications for clinical and epidemiological applications. Part 2. *Clin Chem* **2001,** *47* (3), 418-25.

9.   Ledue, T. B.; Rifai, N., High sensitivity immunoassays for C-reactive protein: promises and pitfalls. *Clin Chem Lab Med* **2001,** *39* (11), 1171-6.

10.   Ockene, I. S.; Matthews, C. E.; Rifai, N.; Ridker, P. M.; Reed, G.; Stanek, E., Variability and classification accuracy of serial high-sensitivity C-reactive protein measurements in healthy adults. *Clin Chem* **2001,** *47* (3), 444-50.

11.   cobas c 111 clinical chemistry analyzer. Roche, Ed. Roche Diagnostics: 2007.

12.   Glavan, A. C.; Christodouleas, D. C.; Mosadegh, B.; Yu, H. D.; Smith, B. S.; Lessing, J.; Fernández-Abedul, M. T.; Whitesides, G. M., Folding Analytical Devices for Electrochemical ELISA in Hydrophobic RH Paper. *Analytical Chemistry* **2014,** *86* (24), 11999-12007.

13.   The enzyme-linked immunosorbent assay (ELISA). *Bull World Health Organ* **1976,** *54* (2), 129-139.

14.   Adedokun, K. A., ELISA_types. Research Gate, 2018.

15.   ACCELERATED EMERGENCY USE AUTHORIZATION (EUA) SUMMARY COVID-19 ELISA IGG ANTIBODY TEST (MOUNT SINAI LABORATORY) Summary, M. S. L. C.-E. I. A. T. E., Ed. FDA, 2020; p 6.

16.   Kimura, A.; Uda, T.; Nakashima, S.; Ikeda, H.; Yasuda, S.; Osawa, M.; Tsuji, T., ABO blood grouping of bloodstains by sandwich ELISA using monoclonal antibody specific for human red cell band 3. *International Journal of Legal Medicine* **1993,** *105* (4), 209-212.

17.   Kundu, S., *BiomedRecent Advances in Immunoassays*. 2014.

18.   Marques, M. P. C.; Szita, N., Bioprocess microfluidics: applying microfluidic devices for bioprocessing. *Current Opinion in Chemical Engineering* **2017,** *18*, 61-68.

19.   Jayne, R. K.; Karakan, M. Ç.; Zhang, K.; Pierce, N.; Michas, C.; Bishop, D. J.; Chen, C. S.; Ekinci, K. L.; White, A. E., Direct laser writing for cardiac tissue engineering: a microfluidic heart on a chip with integrated transducers. *Lab on a Chip* **2021,** *21* (9), 1724-1737.

20.   Mazaafrianto, D. N.; Maeki, M.; Ishida, A.; Tani, H.; Tokeshi, M., Recent Microdevice-Based Aptamer Sensors. *Micromachines (Basel)* **2018,** *9* (5).

21.   Zhang, M.; Desai, T.; Ferrari, M., Proteins and cells on PEG immobilized silicon surfaces. *Biomaterials* **1998,** *19* (10), 953-60.

22.   Singh, R. K.; Tiwari, M. K.; Singh, R.; Lee, J. K., From protein engineering to immobilization: promising strategies for the upgrade of industrial enzymes. *Int J Mol Sci* **2013,** *14* (1), 1232-77.

23.   Tonkinson, J. L.; Stillman, B. A., Nitrocellulose: a tried and true polymer finds utility as a post-genomic substrate. *Front Biosci* **2002,** *7*, c1-12.

24.   Horning, M. P.; Delahunt, C. B.; Singh, S. R.; Garing, S. H.; Nichols, K. P., A paper microfluidic cartridge for automated staining of malaria parasites with an optically transparent microscopy window. *Lab on a Chip* **2014,** *14* (12), 2040-2046.

25.   Ma, J.; Yan, S.; Miao, C.; Li, L.; Shi, W.; Liu, X.; Luo, Y.; Liu, T.; Lin, B.; Wu, W.; Lu, Y., Paper Microfluidics for Cell Analysis. *Advanced Healthcare Materials* **2019,** *8* (1), 1801084.

26.   Sitanurak, J.; Fukana, N.; Wongpakdee, T.; Thepchuay, Y.; Ratanawimarnwong, N.; Amornsakchai, T.; Nacapricha, D., T-shirt ink for one-step screen-printing of hydrophobic barriers for 2D- and 3D-microfluidic paper-based analytical devices. *Talanta* **2019,** *205*, 120113.

27.   Verma, M. S.; Tsaloglou, M. N.; Sisley, T.; Christodouleas, D.; Chen, A.; Milette, J.; Whitesides, G. M., Sliding-strip microfluidic device enables ELISA on paper. *Biosens Bioelectron* **2018,** *99*, 77-84.

28.   Membranes and Filter Papers for Western Blotting. https://www.thermofisher.com/us/en/home/life-science/protein-biology/protein-assays-analysis/western-blotting/transfer-proteins-western-blot/membranes-transfer-buffers-western-blotting.html (accessed 1 May 2021).

29.   Wu, Y.; Liu, J.; Lin, Y.; Weng, R.; Chen, R.; Li, J.; Lv, Z., Diagnosis, Monitoring, and Control of Schistosomiasis-An Update. *J Biomed Nanotechnol* **2018,** *14* (3), 430-455.

30.   Fenollar, F.; Bouam, A.; Ballouche, M.; Fuster, L.; Prudent, E.; Colson, P.; Tissot-Dupont, H.; Million, M.; Drancourt, M.; Raoult, D.; Fournier, P.-E., Evaluation of the Panbio Covid-19 rapid antigen detection test device for the screening of patients with Covid-19. *Journal of Clinical Microbiology* **2020**, JCM.02589-20.

31.   Merino-Amador, P.; Guinea, J.; Muñoz-Gallego, I.; González-Donapetry, P.; Galán, J.-C.; Antona, N.; Cilla, G.; Hernáez-Crespo, S.; Díaz-de Tuesta, J.-L.; Gual-de Torrella, A.; González-Romo, F.; Escribano, P.; Sánchez-Castellano, M. Á.; Sota-Busselo, M.; Delgado-Iribarren, A.; García, J.; Cantón, R.; Muñoz, P.; Folgueira, M. D.; Cuenca-Estrella, M.; Oteo-Iglesias, J., Multicenter evaluation of the Panbio™ COVID-19 Rapid Antigen-Detection Test for the diagnosis of SARS-CoV-2 infection. *medRxiv* **2020**, 2020.11.18.20230375.

32.   Ukena, M., Plastisol vs. Water-based Ink for Textile Printing. Center, P. N. E. A., Ed. 2005.

33. Ibarra, D., Speedball Screen Printing Manual. Products, S. A., Ed. Speedball Art Products Company, 2017; pp 1-41.

34. Koike, A. K., I. Presensitized plate for use in making lithographic printing plate. 1993.

35. Mellan, I. DIAZO CONDENSATION POLYMERS. 21 August 1962, 1962.

36. Basic Chemistry of Photosensitive Emulsions. Limited, P. I., Ed. 2013.

37. Hua, T.-B.; Yang, Q.-Q.; Zou, Y.-Q., Recent Advances in Enantioselective Photochemical Reactions of Stabilized Diazo Compounds. *Molecules* **2019,** *24* (17), 3191.

38. Lee, Y. R. Organic Synthesis Utilizing Diazo Compounds.

39. Poly(vinyl alcohol), MW 78000, 98% hydrolyzed (PVA 78K 98%).

40. Matta, H.; Punj, V.; Kanwar, S. S., An immuno-dot blot assay for detection of thermostable protease from Pseudomonassp. AFT-36 of dairy origin. *Letters in Applied Microbiology* **1997,** *25* (4), 300-302.

41. St John, A.; Price, C. P., Existing and Emerging Technologies for Point-of-Care Testing. *Clin Biochem Rev* **2014,** *35* (3), 155-67.

42. cobas® 8100 automated workflow series. https://diagnostics.roche.com/us/en/products/systems/cobas_-8100-automated-workflow-series.html (accessed 4 May 2021).

43. Marques, M. P.; Szita, N., Bioprocess microfluidics: applying microfluidic devices for bioprocessing. *Curr Opin Chem Eng* **2017,** *18*, 61-68.

44. Ansari, M. I. H.; Hassan, S.; Qurashi, A.; Khanday, F. A., Microfluidic-integrated DNA nanobiosensors. *Biosens Bioelectron* **2016,** *85*, 247-260.

45.   Cardiovascular Disease: Risk Assessment With Nontraditional Risk Factors.

https://www.uspreventiveservicestaskforce.org/uspstf/recommendation/cardiovascular-

disease-screening-using-nontraditional-risk-assessment (accessed 1 May 2021).

46.   Johns, C. New guideline recommends CAC scoring when there is uncertainty

regarding benefit from statins. https://scct.org/news/427405/New-guideline-

recommends-CAC-scoring-when-there-is-uncertainty-regarding-benefit-from-

statins.htm.

47.   Geoffrey D. Barnes, M., MSc, FACC Screening for PAD and CVD Risk With ABI:

USPSTF Recommendation. https://www.acc.org/latest-in-cardiology/ten-points-to-

remember/2018/07/11/14/31/screening-for-peripheral-artery-disease-and-

cardiovascular-

disease#:~:text=The%20American%20College%20of%20Cardiology,of%20PAD%2C%

20and%20adults%20%3C50 (accessed 1 May 2021).

48.   Liang, K.; Chow, C.-W.; Liu, Y., RGB visible light communication using mobile-

phone camera and multi-input multi-output. *Opt. Express* **2016,** *24* (9), 9383-9388.

49.   Opal Medical Apps. https://opalmedapps.com/.

50.   Hulsen, T.; Jamuar, S. S.; Moody, A. R.; Karnes, J. H.; Varga, O.; Hedensted, S.;

Spreafico, R.; Hafler, D. A.; McKinney, E. F., From Big Data to Precision Medicine.

Frontiers in Medicine **2019,** *6* (34).

51.   O'Connor, A. How Artificial Intelligence Could Transform Medicine.

52.   Sinha, P.; Matthay, M. A.; Calfee, C. S., Is a "Cytokine Storm" Relevant to

COVID-19? *JAMA Internal Medicine* **2020,** *180* (9), 1152-1154.

53.   Samprathi, M.; Jayashree, M., Biomarkers in COVID-19: An Up-To-Date Review. *Front Pediatr* **2020,** *8*, 607647.

54.   Ombrello, M. J.; Schulert, G. S., COVID-19 and cytokine storm syndrome: are there lessons from macrophage activation syndrome? *Transl Res* **2021,** *232*, 1-12.

55.   Mueller, A. A.; Tamura, T.; Crowley, C. P.; DeGrado, J. R.; Haider, H.; Jezmir, J. L.; Keras, G.; Penn, E. H.; Massaro, A. F.; Kim, E. Y., Inflammatory Biomarker Trends Predict Respiratory Decline in COVID-19 Patients. *Cell Rep Med* **2020,** *1* (8), 100144.

56.   Gómez-Pastora, J.; Weigand, M.; Kim, J.; Wu, X.; Strayer, J.; Palmer, A. F.; Zborowski, M.; Yazer, M.; Chalmers, J. J., Hyperferritinemia in critically ill COVID-19 patients - Is ferritin the product of inflammation or a pathogenic mediator? *Clin Chim Acta* **2020,** *509*, 249-251.

57.   Yao, Y.; Cao, J.; Wang, Q.; Shi, Q.; Liu, K.; Luo, Z.; Chen, X.; Chen, S.; Yu, K.; Huang, Z.; Hu, B., D-dimer as a biomarker for disease severity and mortality in COVID-19 patients: a case control study. *J Intensive Care* **2020,** *8*, 49.

58.   Stringer, D.; Braude, P.; Myint, P. K.; Evans, L.; Collins, J. T.; Verduri, A.; Quinn, T. J.; Vilches-Moraga, A.; Stechman, M. J.; Pearce, L.; Moug, S.; McCarthy, K.; Hewitt, J.; Carter, B., The role of C-reactive protein as a prognostic marker in COVID-19. *Int J Epidemiol* **2021**.

59.   Multiplex Human Cytokine ELISA Kits. (accessed 1 May 2021).

APPENDIX A: Inlet Layer, Verma Design
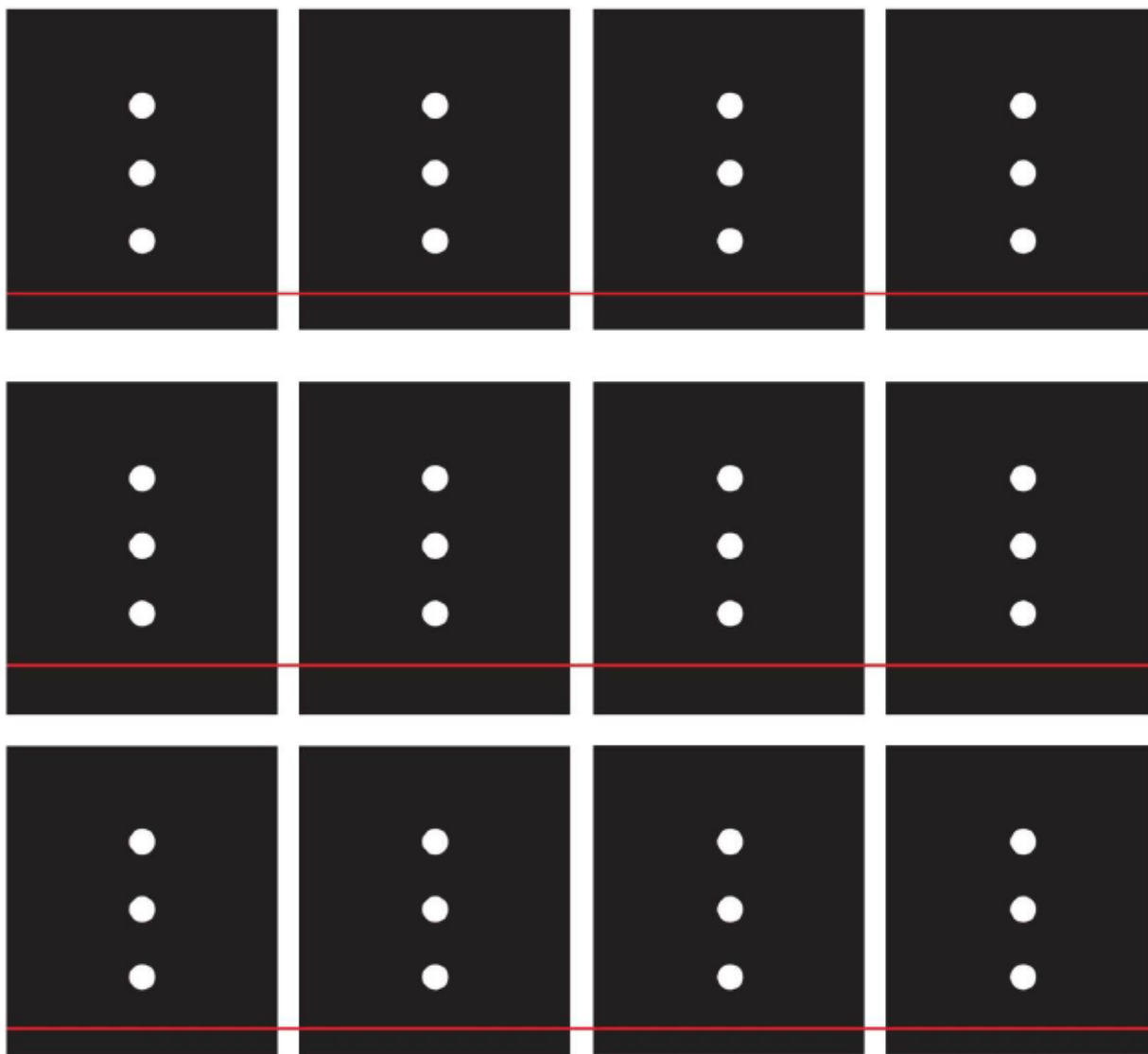
This pattern is to be printed onto chromatography paper.

APPENDIX B: Splitting Layer, Verma Design
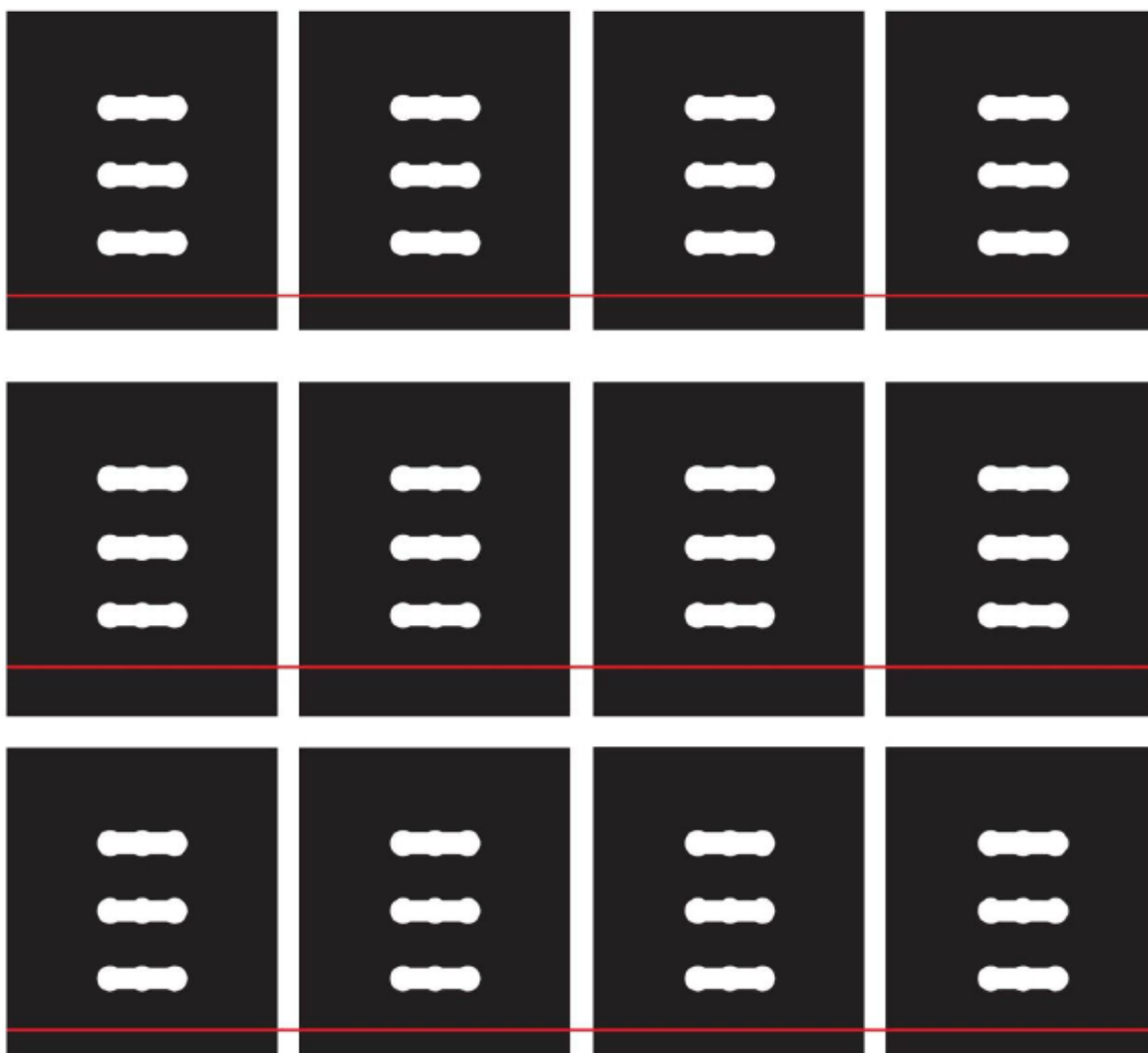
This pattern is to be printed onto chromatography paper.

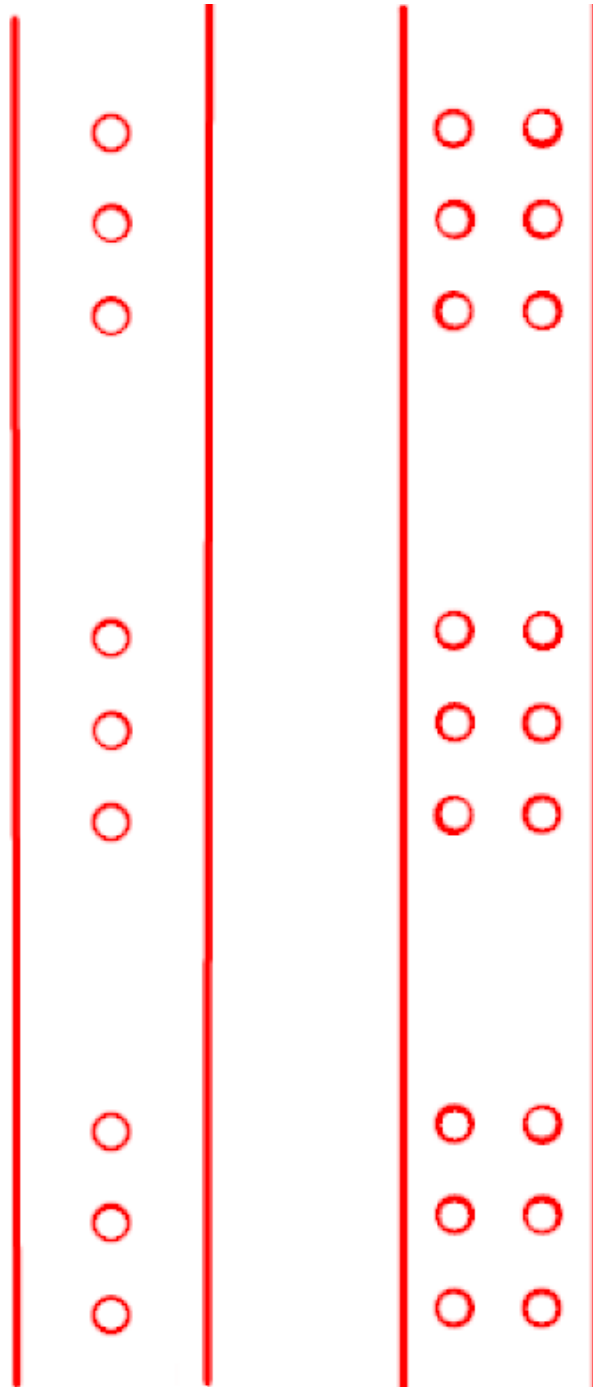**APPENDIX C: Isolation and Functional Layer, Verma Design**
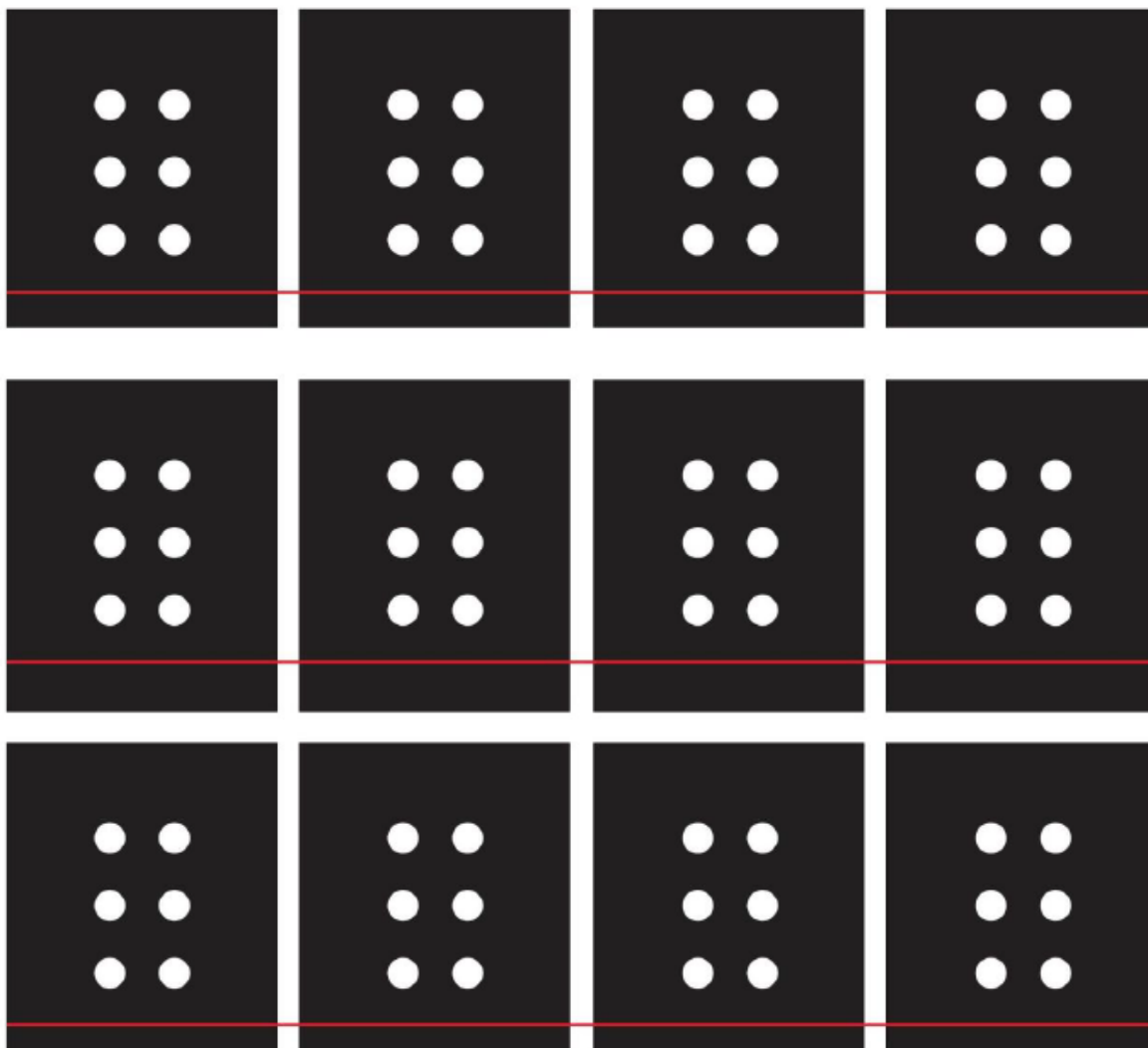
This pattern is to be printed onto chromatography paper.

APPENDIX D: Sliding Dock, Verma Design
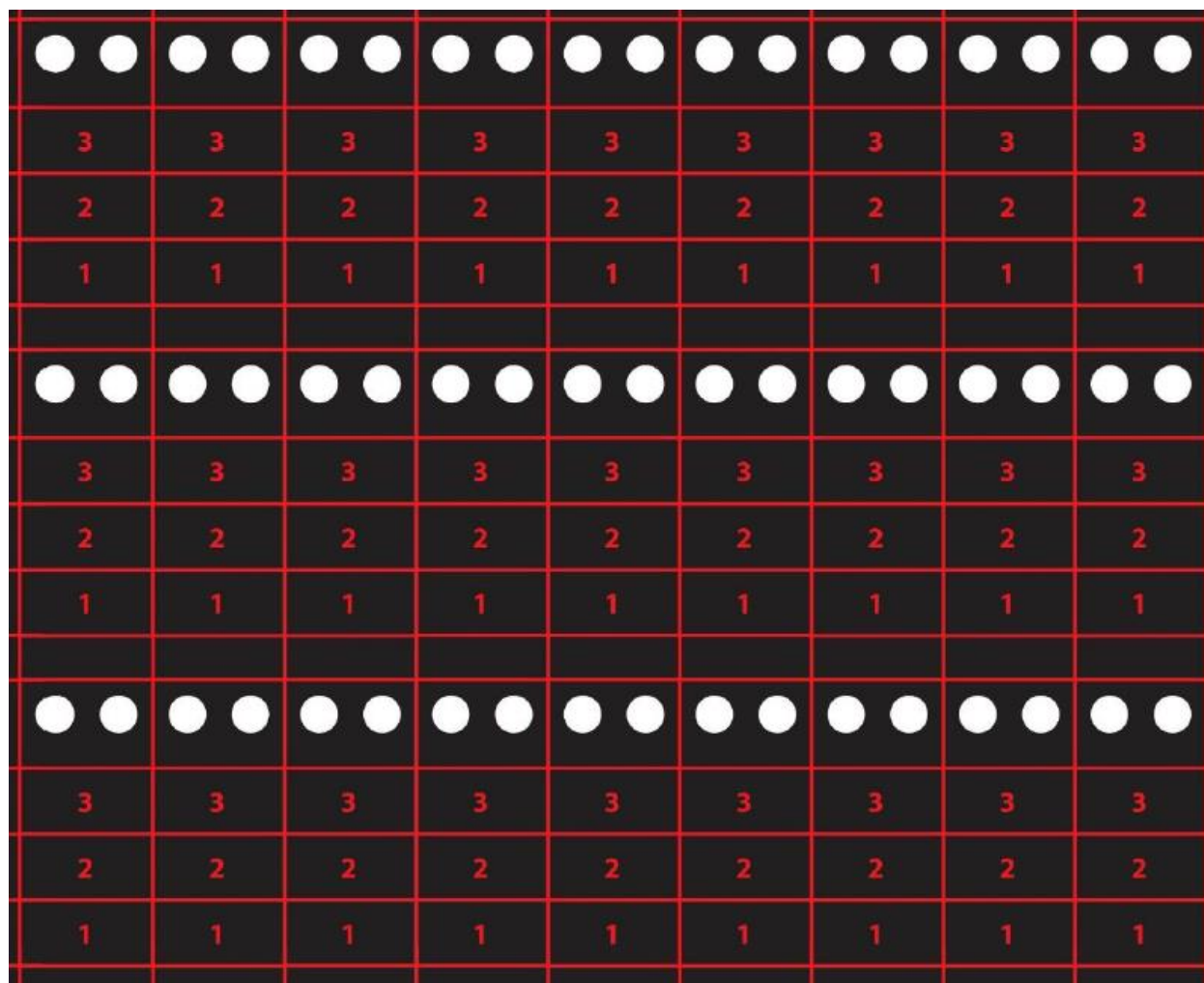
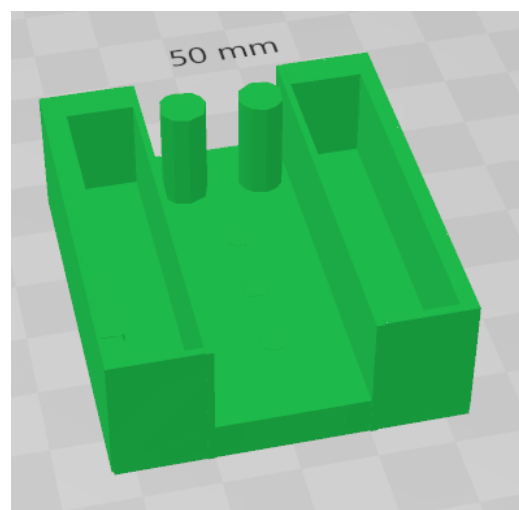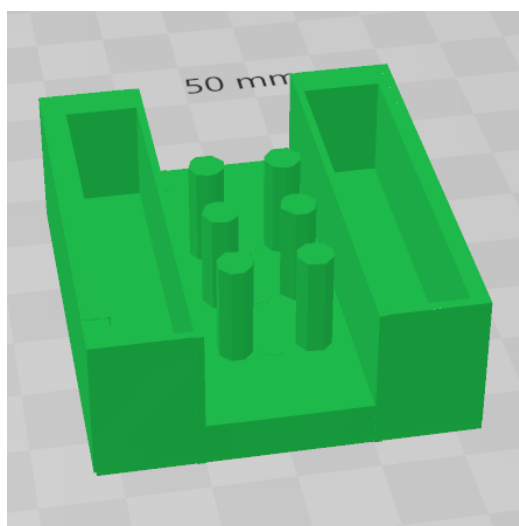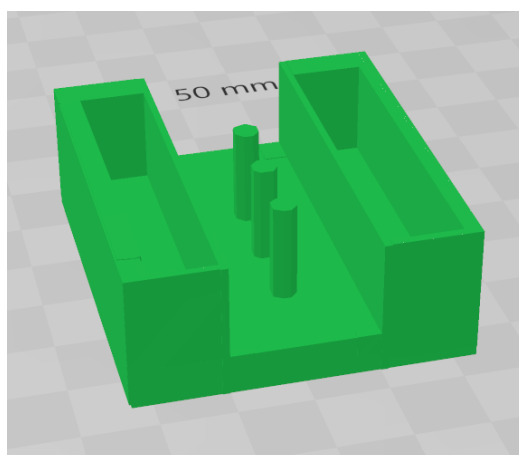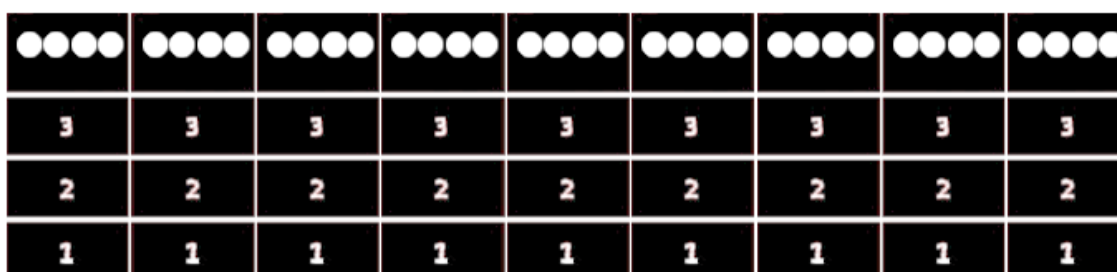

This pattern is to be printed onto chromatography paper.

APPENDIX E: Sensing Dock, Verma Design

This pattern is to be printed onto nitrocelulose paper.

APPENDIX F: Laser Cutter File

This file is intended for the Versa Cutter in the Digital Lab at Bard College. Lines indicate clean cuts. This is to be cut out of the double sided tape used in µPAD fabrication.

APPENDIX G: Tape Aligners for µPAD Fabrication

The images above are STL files (ready for 3D printing) used to properly align the double sided tape with the hydrophobic barriers printed on the inlet layer (top), functional/isolation layer (middle), and sliding dock (bottom).

APPENDIX H: Inlet Layer, Novel Design
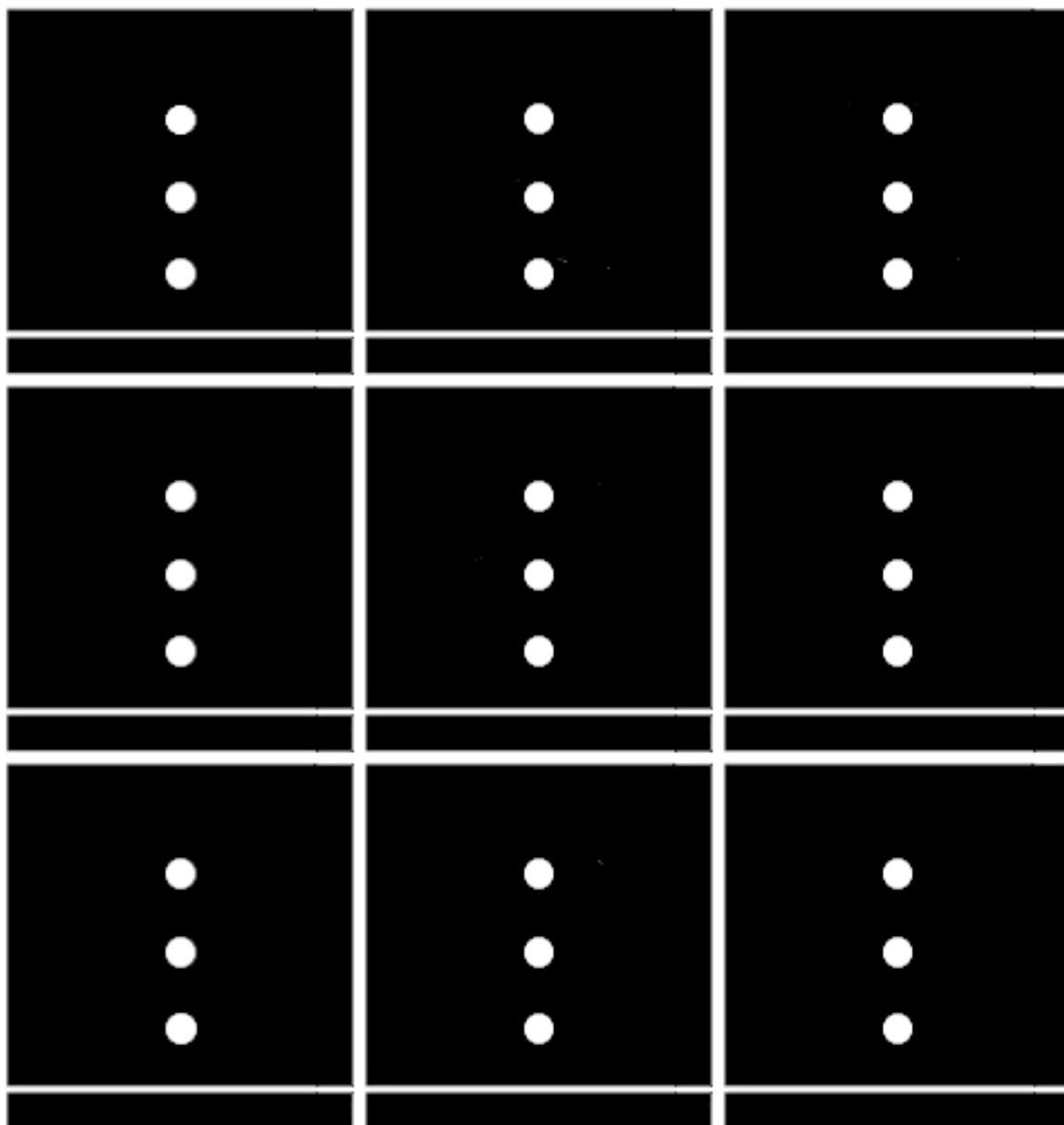
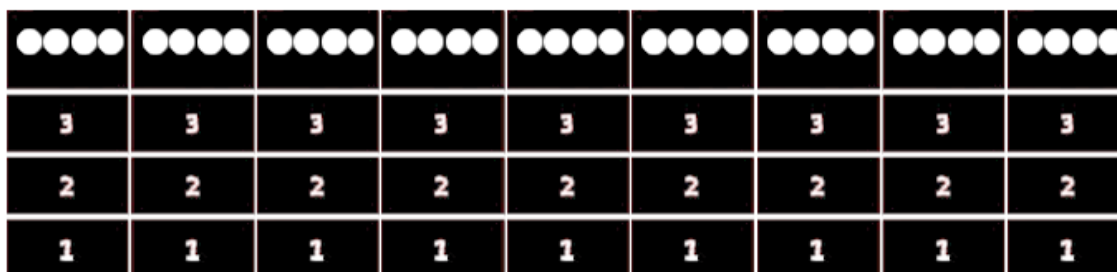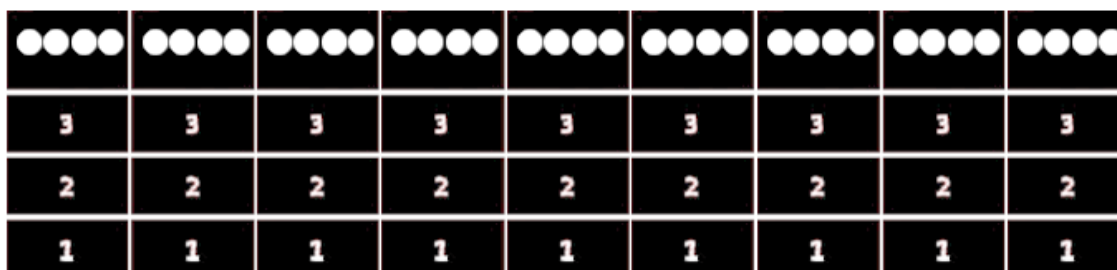This pattern is to be printed onto chromatography paper.

APPENDIX I: Splitting Layer, Novel Design
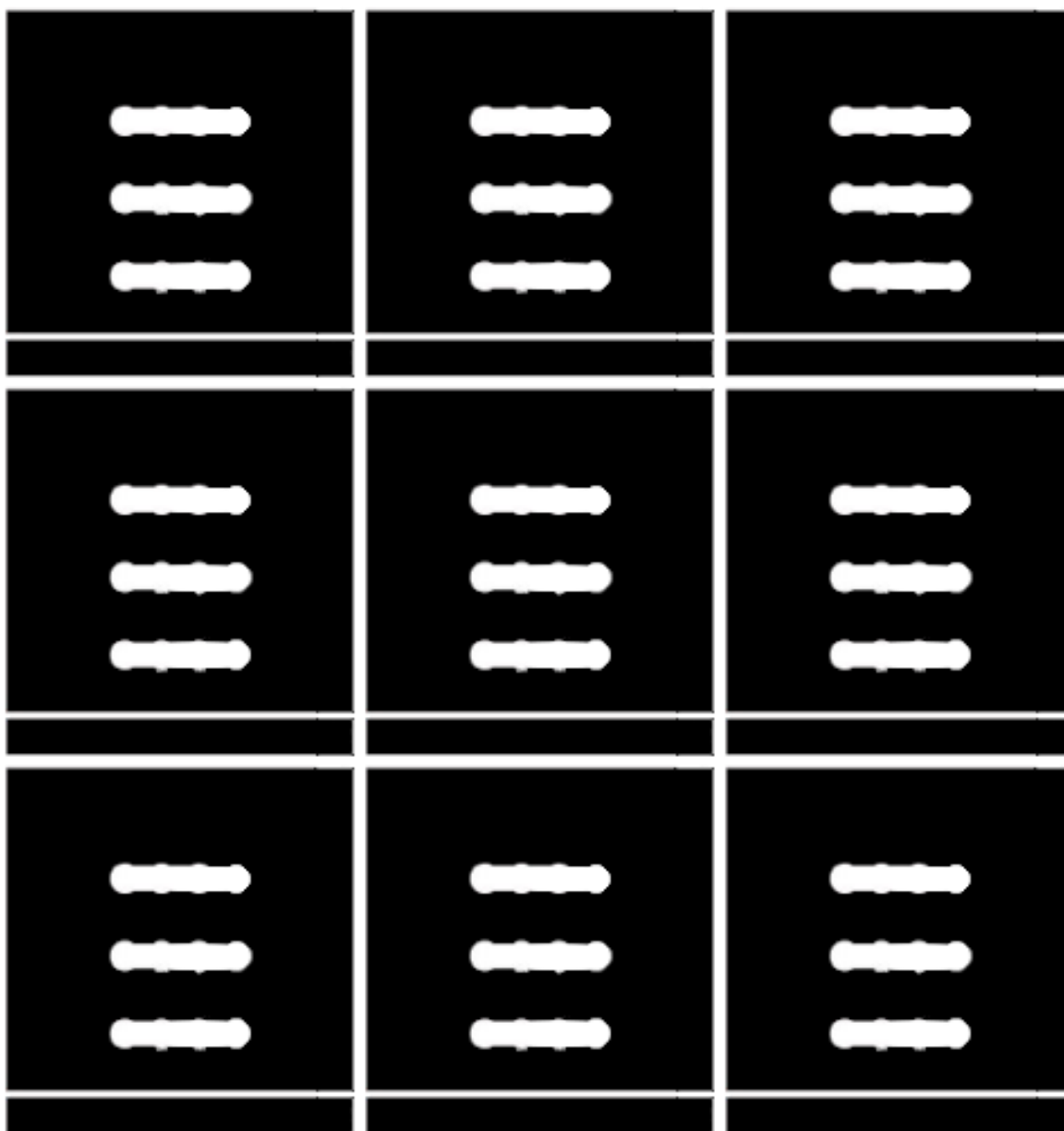
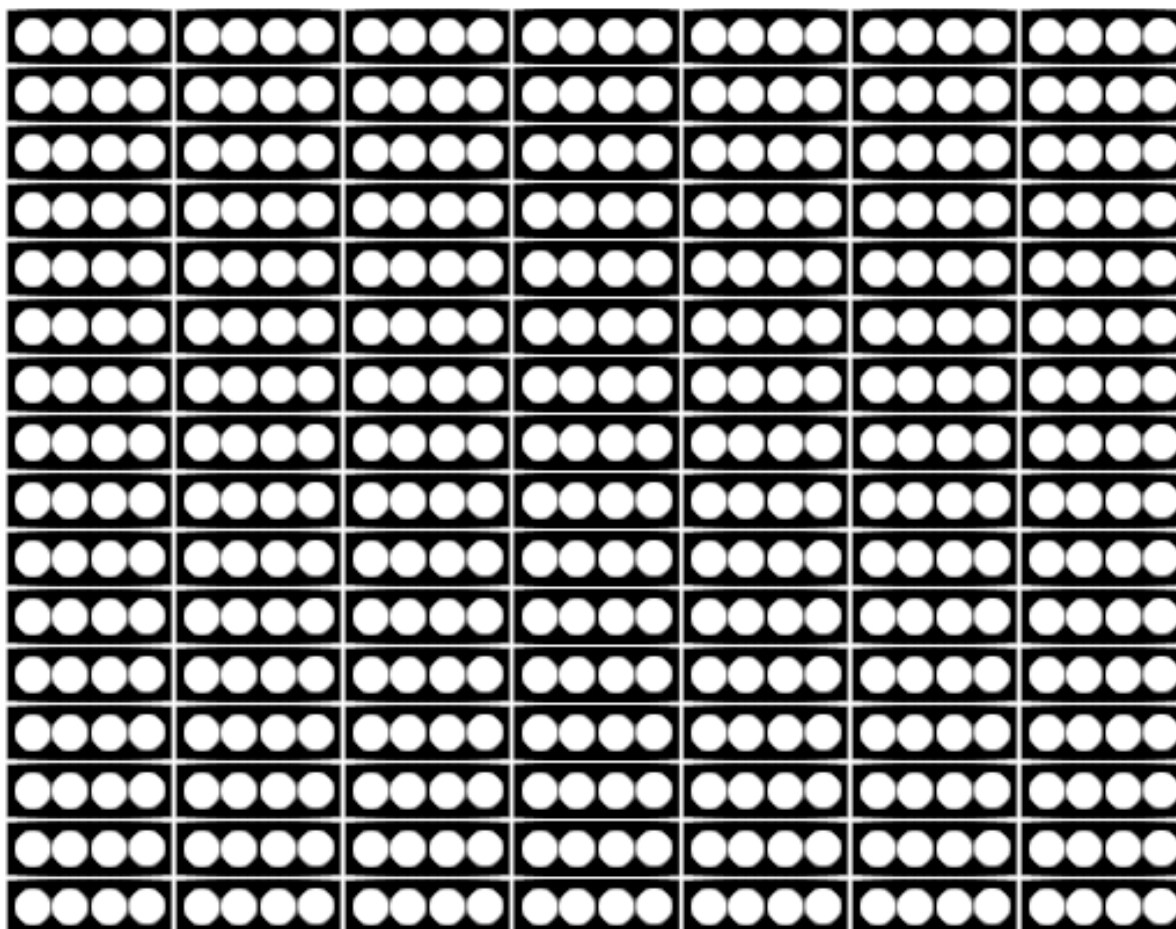This pattern is to be printed onto chromatography paper.

APPENDIX J: Isolation and Functional Layer, Novel Design
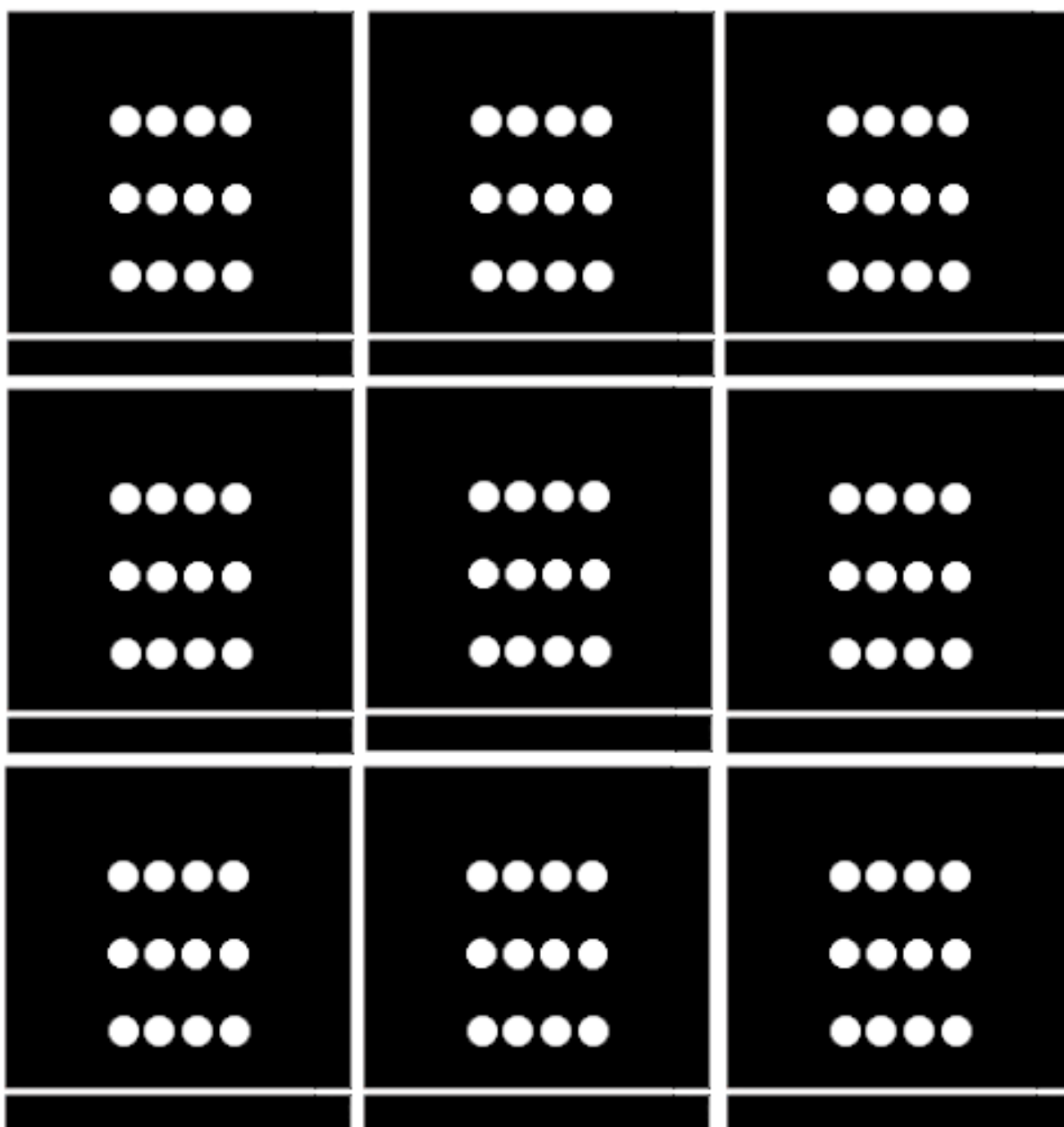
This pattern is to be printed onto chromatography paper.

APPENDIX K: Sliding Dock, Novel Design

This pattern is to be printed onto chromatography paper.

APPENDIX L: Sensing Dock, Novel Design

This pattern is to be printed onto nitrocellulose paper.